Ore Geology Reviews 112 (2019) 103018

Contents lists available at ScienceDirect

Ore Geology Reviews

journal homepage: www.elsevier.com/locate/oregeorev

Delimiting geochemical anomalies in the exploration of covered deposits with multifractal methods and using stream sediment data from the Iberian Pyrite Belt, Southwest Iberia

Mário A. Gonçalves[a,b,*], A. Mateus[a,b]

[a] Departamento de Geologia, Faculdade de Ciências da Universidade de Lisboa, Edifício C6, Piso 4, Campo Grande, 1749-016 Lisboa, Portugal
[b] IDL – Instituto Dom Luíz, Faculdade de Ciências da Universidade de Lisboa, Edifício C1, Piso 1, Campo Grande, 1749-016 Lisboa, Portugal

ARTICLE INFO

Keywords:
Faint geochemical anomalies
Singularity
Multifractals
Iberian Pyrite Belt
Mineral exploration under cover

ABSTRACT

The Iberian Pyrite Belt (IPB) is a world-class province of Upper Paleozoic age for volcanic- and shale-hosted massive sulfides that includes 5 of the 10 supergiant (> 150 Mt) deposits of their kind in the World. The volcano-sedimentary sequences hosting the ores are locally exposed, commonly covered by flysch-type successions of variable thickness (the Baixo Alentejo Flysch Group, BAFG) as a result of primary (sedimentary) features and superimposed effects due to Variscan folding and tectonic stacking. In addition and when affected by late-developed geomorphic depressions, the exhumed Paleozoic basement is also capped by Meso-Cenozoic sediments. The total thickness of cover sequences on top of the litho-stratigraphic sequence of interest can reach 100's of meters, creating problems for mineral exploration.

A large stream sediment (multi-element) geochemical database for the IPB was done in the 90's during a wide-ranging regional survey. This database was reassessed by means of multifractal methods in view of their faculty to enhance the detection of faint geochemical anomalies and provide geochemical indicators to deep buried ore systems. Several anomalies were detected, namely for Cu, Zn, and Co along NW-SE to WNW-ESE trends. The main anomalous geochemical trends identified include zones that: (i) extend along the Mira Formation of BAFG, opening for the first time two non-traditional areas for further exploration studies; (ii) run along the boundary between the Mira and Mértola Formations of BAFG, probably related to different geochemical signatures and late-developed, fault-controlled, epigenetic ore systems; and (iii) overlap windows of volcanic-sedimentary sequences within the Cenozoic detrital cover and the site below which the deep buried deposit of Lagoa Salgada is located.

1. Introduction

The search for concealed ore deposits has always been a challenging and demanding task in mineral exploration. Success has depended on various innovations in data acquisition and processing, involving a multitude of exploration techniques (geochemical, geophysical, mineralogical, etc.) combined with integrative models that consider the geological attributes of ore deposits and their geodynamic framework (McCuaig et al., 2010; McCuaig and Hronsky, 2014; Lazwcka, 2014; Hagemann et al., 2016; Huston et al., 2016). The pressure for new discoveries has also been increasing as a result of the fast growing consumption of minerals in general and widespread use of high-tech metals in particular, and limited reuse, recycling and substitution practices (Mason et al., 2011; Humphreys, 2013; Vidal et al., 2013; Moran et al., 2014; Fortier et al., 2018). Accordingly, the common re-assessment of existing databases available for known mineral provinces has been receiving renewed attention in the expectation they might hold relevant overlooked information. For such purpose, however, the reasoning and the tools involved in data handling should differ from those used in the past.

The Iberian Pyrite Belt (IPB) in SW Iberia is a well-known major province hosting world-class massive sulfide (volcanic- and shale-hosted) ore systems (Tornos, 2006). In this belt, some high-quality resources were discovered in the last 60 years by geological/geophysical methods at depths in excess of 100 m, as the case of the giant deposit of Neves-Corvo (Leca et al., 1983; Relvas et al., 2002 and references therein). Target commodities in the IPB extend beyond the main base metals (Cu and Zn), and include Sn and other metals hosted in some ore

* Corresponding author at: Departamento de Geologia, Faculdade de Ciências da Universidade de Lisboa, Edifício C6, Piso 4, Campo Grande, 1749-016 Lisboa, Portugal.
E-mail address: mgoncalves@ciencias.ulisboa.pt (M.A. Gonçalves).

https://doi.org/10.1016/j.oregeorev.2019.103018
Received 6 August 2018; Received in revised form 4 April 2019; Accepted 12 July 2019
Available online 15 July 2019
0169-1368/

types such as those within the Neves-Corvo deposit (Serranti et al., 2002; Pinto et al., 2014; Carvalho et al., 2018).

Mineral exploration activities in IPB have been carried out since (at least) Roman times, mostly surveying: (i) exposures of the Uppermost Devonian to Mid-Carboniferous volcano-sedimentary sequences, the prevalent host of sulfide ores; and (ii) lateral extensions of these sequences covered by Upper Carboniferous flysch-type successions and/or by Meso-Cenozoic sediments lately deposited over the exhumed Paleozoic basement. The knowledge systematically accumulated over decades led to a series of criteria that are routinely used in exploration endeavors and proved to be successful, particularly in many brownfield frameworks. Nonetheless, in large part of the IPB western domains, the piles covering the volcano-sedimentary sequences can often reach 100′s of meters, putting additional difficulties in the recognition of anomalies related to geochemical dispersion from ore systems at depth, even combining results gathered from complementary geophysical methods. At a regional scale, the use of geochemical exploration approaches in the IPB is quite limited because of the difficulty in combining historically available datasets with different detection limits for example (Grunsky, 2010; Yilmaz et al., 2017), each one usually representing the environments enclosing known ore systems or promising targets.

During the 90′s, the exploration company Sociedade Mineira Rio Artezia, (subsidiary of the Rio Tinto Group) undertook a major stream sediment campaign covering almost all of the South Portuguese Zone (SPZ), the southernmost geotectonic unit of the Variscan fold belt in the Iberian Peninsula hosting the IPB. The resulting (multi-element) geochemical database is, to our knowledge, the sole catalogue available for the SPZ (and IPB) that: (i) includes a large number of samples covering areas made of Upper Carboniferous flysch-type successions and Meso-Cenozoic sediments above the volcano-sedimentary sequences of prevailing interest; and (ii) all the samples were handled and subjected to the same analytical routines, thus generating a consistent collection of element concentration values of regional meaning. This geochemical database, although previously studied (Feliciano et al., 2008) still holds some potential information regarding faint anomalies and other geochemical indicators that can drive further exploration endeavours in targeted areas for the search of massive sulfide orebodies under the Upper Carboniferous flysch and/or Meso-Cenozoic sedimentary cover.

In the past decades a wealth of research papers have been applying methods based on multifractal theory to identify and separate distinctive source signals from datasets which may be ultimately related to mineralizing systems. The first, most commonly used and successfully tested in a wide range of situations is the concentration-area (C-A) method (Cheng et al., 1994) which provides anomalous thresholds that can be related to the geological background. Other methods have been proposed such as the concentration-distance based on Mandelbrot's radial distribution function, spectrum-area using filtering techniques, and singularity mapping (Cheng, 2007; Cheng and Agterberg, 2009; Cheng et al., 2000; Li et al., 2003; Liu et al., 2017; Yang et al., 2015; Chen et al., 2007; Zuo, 2011; Zuo and Wang, 2016). More recently, some of these methods were combined with stochastic simulation in order to provide a probabilistic output of the delineated anomalies (e.g., Rantitsch, 2001; Yousefi and Carranza, 2015; Sadeghi et al., 2015; Wang and Zuo, 2018).

Several studies applied the C-A method to mineralizing systems in the Variscan fold belt (Gonçalves et al., 2001; Arias et al., 2012; Jesus et al., 2013), some to the IBP (Luz et al., 2012, 2014a,b). The C-A method is strongly influenced by regional scale structures and not always resolve adequately the intended separation, requiring denser sampling to outline smaller zones with anomalous geochemistry. Another difficulty inherent to the C-A method is that thresholds embody all the areas above a given elemental concentration, thus grouping together faint anomalies potentially related to ore systems and natural variations due to intrinsic compositional heterogeneities showed by sediments and rocks. Singularity mapping has been proposed as a tool to overcome these difficulties (Zuo and Wang, 2016; Wang and Zuo, 2018; Wang et al., 2018; Gonçalves et al., 2018) through the measurement of local enrichments or depletions with respect to a neighbouring area (controlled with the window side length to compute the singularity index). Therefore, variations in concentration perceived as not relevant can be strongly outlined because of the neighboring geochemical pattern.

The objective of this paper is to define new targets for exploration never before considered in the years of past exploration history in the SPZ using stream sediment geochemical data, both with the C-A method and singularity index. Additionally, the results have been de-convoluted with the intention to separate contributions from different geological units and to assess the sensitivity of the singularity index with respect to a high background noise as expected for faint anomalies above deep buried ore systems. Anomalous geochemical patterns identified by the C-A/singularity approach are evaluated, in particular those associated with the Upper Carboniferous flysch-type successions and/or the Meso-Cenozoic sediments, to establish (i) whether such anomalies are of any significance at the regional scale, (ii) the spatial relationship to possible signals from deposits seated beneath that cover of variable composition, structural disposition and thickness and (iii) consider mechanisms or processes to explain the development of geochemical patterns in stream sediment samples.

2. Geological setting

The SPZ is the southernmost geotectonic unit of the Variscan Fold Belt in the Iberian Peninsula, representing a terrane of Avalonian affinity (Matte and Ribeiro 1975; Dias and Ribeiro, 1995; Oliveira et al., 1979; Quesada 1991, 1998; Ribeiro et al., 2007). The northern border of this geotectonic unit is outlined by a major suture, currently traced by the Ferreira-Ficalho Thrust Fault (Mateus et al., 1999; da Silva et al., 2007; Jesus et al., 2007; Ribeiro et al., 2010), separating it from the Ossa-Morena Zone (OMZ) in the Iberian Terrane of Gondwanan affinity (Fig. 1; Fig. S1 in the SI file for sub-divisions of the main units). The contacting units of the OMZ correspond to a suite of stretched and highly dismembered mafic/ultramafic rocks that form the Beja-Acebuches Ophiolite Complex (BAOC) (Fonseca and Ribeiro 1993; Quesada et al., 1994; Figueiras et al., 2002).

The SPZ is usually divided into four main domains that, from NE/NNE to SW, known as: (i) the Pulo do Lobo Terrane (PLT); (ii) the Iberian Pyrite Belt (IBP); (iii) the Baixo Alentejo Flysch Group (BAFG); and (iv) the Southwest Sector, embracing the Bordeira and Aljezur domains having similar lithological features and age (Oliveira et al., 1985; Pereira, 1999; Oliveira et al., 2013).

The PLT, interpreted as an accretionary prism evolved during the northward subduction of an oceanic plate under the OMZ, is intensely deformed by interfering tight SW-vergent folds and thrusts (Ribeiro et al., 1990, 2010; Fonseca et al., 1999; Oliveira et al., 2013; Pereira et al., 2018).

The IPB includes from bottom to top (Van den Boogaard, 1963; Silva et al., 1990; Oliveira 1990; Oliveira et al., 2005, 2013; Rosa et al., 2006, 2008, 2009; Pereira et al., 2007):

1. The Phyllite-Quartzite Group (PQG) of Upper Devonian age, comprising mostly a siliciclastic sequence made of phyllites, quartzites, and *meta*-quartzwackes.
2. The Volcanic-Sedimentary Complex (VSC), including a diachronic sequence of Uppermost Devonian to Mid-Carboniferous siliciclastic rocks (mostly metapelites) interbedded with volcaniclastic units and/or intruded by igneous bodies. The volcanics comprise felsic derivatives (rhyolitic to rhyodacitic) that, according to present exposures, dominate over mafic rocks (Routhier et al., 1980; Munhá, 1983a; Leistel et al., 1994; Mitjavilla et al., 1997; Thiéblemont et al., 1998; Carvalho et al., 1999; Rosa et al., 2004, 2006; Codeço et al., 2018). The VSC sequences record the progression of the activity related to several volcanic centers as determined by the opening of

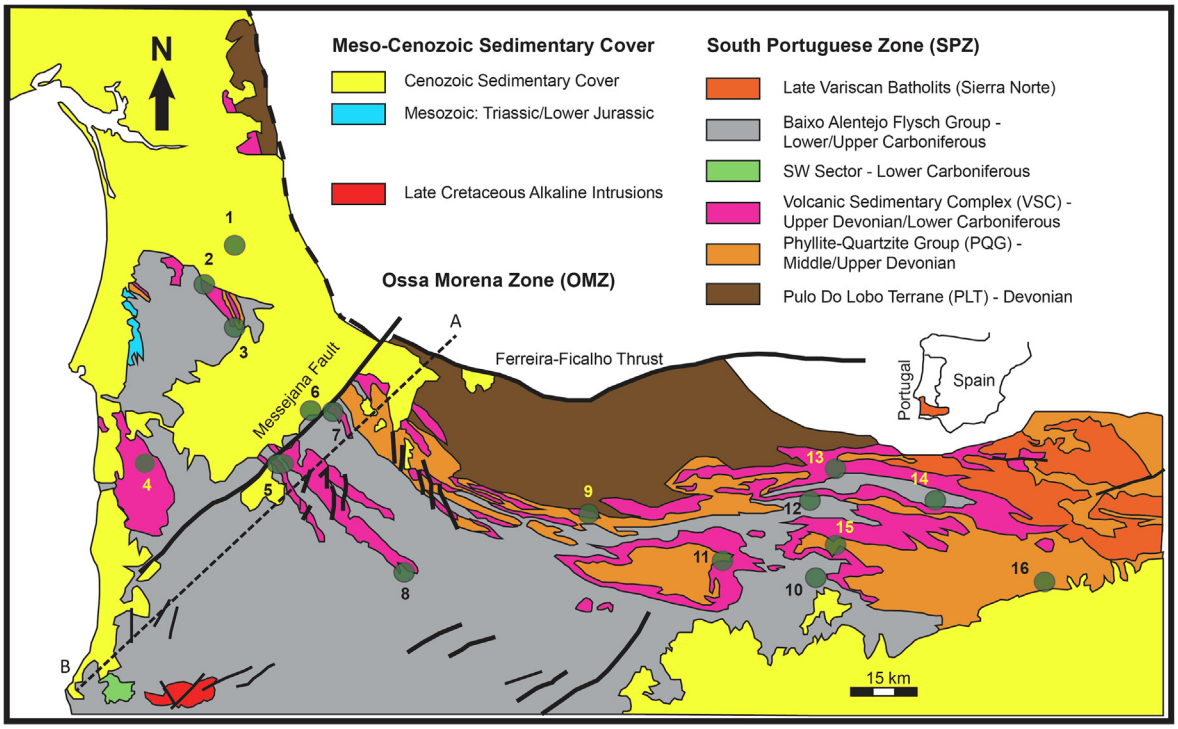

Fig. 1. Simplified geological map of the South Portuguese Zone. Detailed description of the lithological units is given in the text. Green circles indicate the location of VHMS Portuguese deposits (1–9) and selected main deposits in Spain (10–16). 1 – Lagoa Salgada*; 2 – Caveira; 3 – Lousal; 4 – Salgadinho (near Cercal); 5 – Montinho; 6 – Gavião* (extension of Aljustrel NW of the Messejana Fault); 7 – Aljustrel; 8 – Neves Corvo*; 9 – S. Domingos; 10 – Masa Valverde; 11 – Tharsis; 12 – La Zarza; 13 – Aguas Teñidas; 14 – Riotinto; 15 – Sotiel; 16 – Aznalcollar. * – buried deposits under sedimentary cover. Inset of the Iberian Peninsula shows the area representation of the map. The Messejana Fault and the Ferreira-Ficalho Thrust are indicated. For a more detailed geological map of the SPZ in the Portuguese sector, see Fig. S1 in the SI file. Dashed line A-B marks the location of the geological cross-section of Fig. 2. (For interpretation of the references to colour in this figure legend, the reader is referred to the web version of this article.)

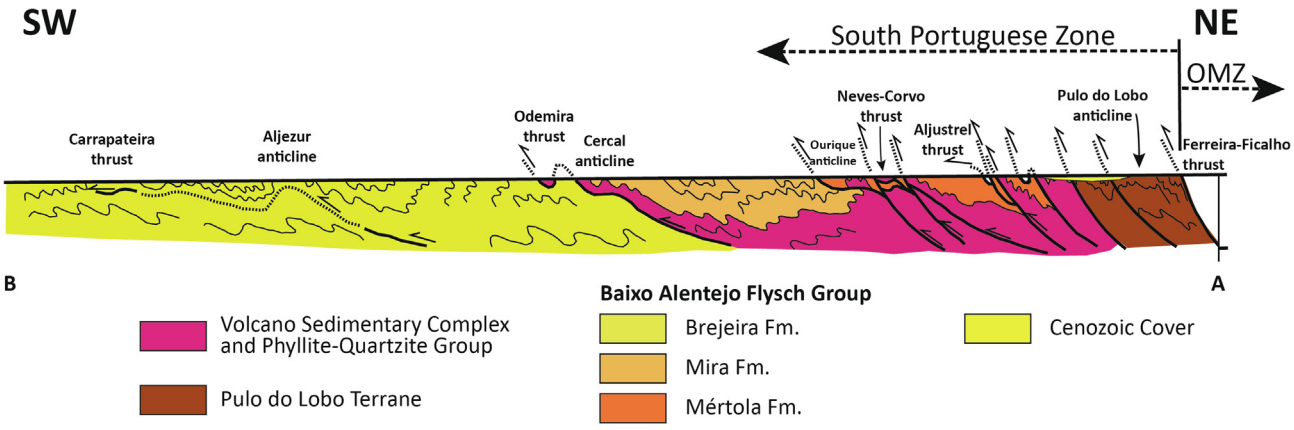

Fig. 2. General geological cross-section of the South Portuguese Zone, showing the structure of the IPB with imbricated thrusts, and the positioning of the Mértola and Mira Formations of the BAFG relative to the VCS. Note that for the sake of simplicity, VSC and PQG lithologies were grouped, and colours used for the BAFG differ for better reading. Adapted from Ribeiro et al. (2007).

transtensional basins during the Variscan cycle. The felsic volcanic centers were mostly constituted by lavas, domes, and crypto-domes of rhyolitic and rhyodacitic affinity, to which most massive sulfide deposits are temporally and spatially associated. These rocks result from partial melting of crustal materials in a high thermal gradient environment which is suggested to have been provided by the mafic volcanism (Munhá, 1983a, Rosa et al., 2004, 2006; Codeço et al., 2018).

The BAFG is a succession of flysch-like sediments divided into three main formations of Upper Carboniferous age, from NE to SW: Mértola, Mira, and Brejeira, (Oliveira et al., 2013). Lithic clasts in *meta*-greywackes of the Mértola Formation often correspond to rock types forming the VSC (Oliveira et al., 1993; Oliveira et al., 2013). The depositional history and provenance of these formations has been recently studied and discussed (Oliveira et al., 2013; Jorge et al., 2013; Rodrigues et al., 2015).

Variscan metamorphism is generally in the prehnite-pumpllyite facies progressing to greenschist facies towards the northern border of IPB and PLT (Munhá, 1979; 1981; 1983b, 1990; Abat et al., 2001). The PQG and VSC also preserve evidence of pre-Variscan regional alteration due to oceanic metasomatism that led to extreme alteration of the mafic units to spilites (Munhá and Kerrich, 1980).

While the PLT records an earlier deformation phase (late Devonian)

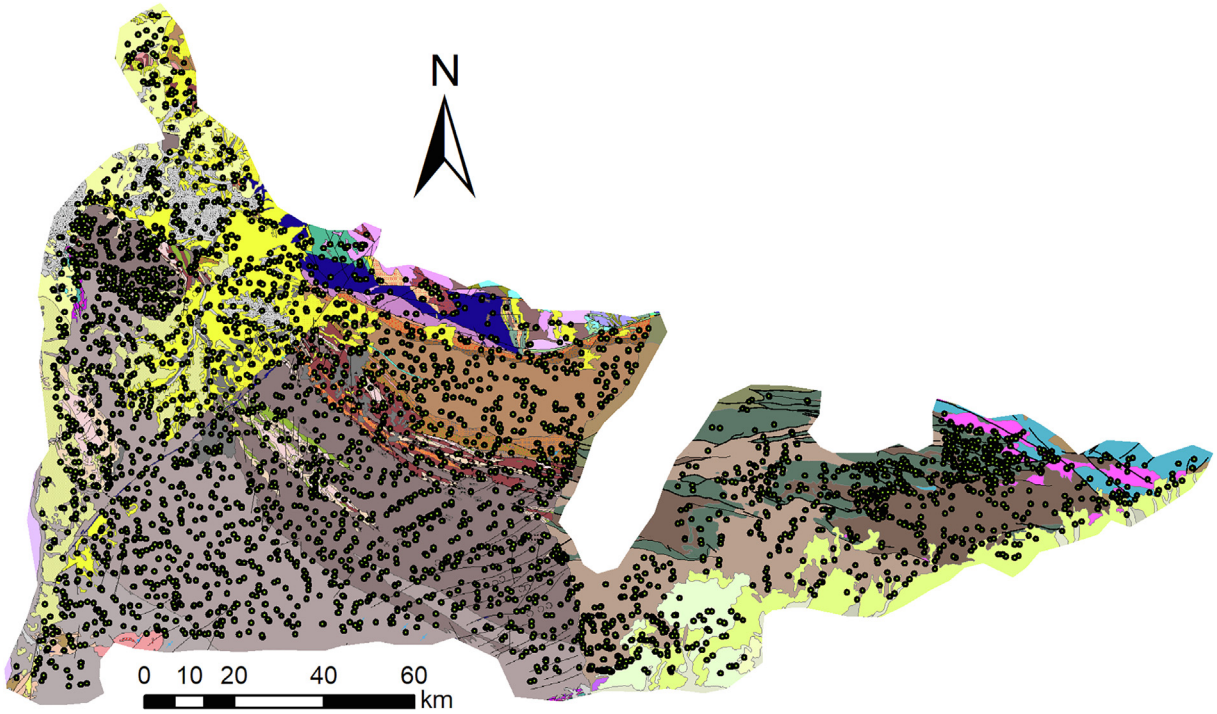

Fig. 3. Stream sediment sample locations. Projection over the geological map of Portugal (1:500,000; LNEG repository; WMS Server http://geoportal.lneg.pt/geoportal/mapas/index.html?servico=CGP500k/MapServer/WMSServer; Fig. S1) and Iberian Peninsula (1:1,000,000; IGME repository; WMS Server http://mapas.igme.es/gis/services/Cartografia_Geologica/IGME_Geologico_1M/MapServer/WMSServer) in the Spanish side.

with respect to the remaining domains of the SPZ, its major structuring occurs during the tectonic inversion of the basin under a transpressive regime and completed in late Carboniferous times (Ribeiro et al., 1983, 2010; Silva et al., 1990; Quesada, 1998). This resulted in a progression of the Variscan deformation from NE to SW with the development of folds and thrusts, some recorded as being *syn*-sedimentary in the BAFG, providing the overall development of a thin-skinned tectonic style (Silva et al., 1990). Consequently, structural arrays of high complexity are locally developed, disturbing variably the stratigraphic sequence and promoting the stacking of slices involving sections of PQG, VSC and BAFG (Fig. 2) with relevant implications in mineral exploration (Leca et al., 1983; Marignac et al., 2003; Inverno et al., 2015b; Martín-Izard et al., 2016). Displacements of variable magnitude related to the Late-Variscan network of strike-slip fault zones (Arthaud and Matte, 1975; Marques et al., 2002; Dias et al., 2017), as well as the correlative hydrothermal activity related to multiple seismic cycles, are also meaningful to the structural arrays of interest for mineral exploration (Carvalho et al., 1971; Mateus, 2001). Furthermore, after exhumation of the Paleozoic basement, many of these strike-slip faults were subjected to considerable reactivation (Arthaud and Matte, 1975; Ribeiro et al., 1990; Tornos et al., 2000; Silva et al., 2008), thus contributing to the rejuvenation of relief during the Alpine Cycle and confining the local advancement of sedimentation processes that took place in Meso-Cenozoic times.

2.1. VMS mineralization and mineral exploration in the IPB

The IPB hosts more than 90 massive sulfide deposits scattered in Portugal and Spain varying in tonnage from 1 to > 300 Mt. There are 14 world-class (> 32 Mt) deposits, some of which are classified as giant (> 100 Mt), such as Riotinto and La Zarza in Spain, and Aljustrel and Neves Corvo in Portugal (Fig. 1). Most are pyrite-rich but 11 deposits can be considered large with respect to Cu-Zn-Pb reserves (Barriga, 1990; Barriga and Fyfe, 1988; Leistel et al., 1998; Sáez et al., 1996, 1999; Tornos et al., 2000; Tornos and Heinrich, 2008; de Oliveira et al., 2011; Inverno et al., 2015a; Martín-Izard et al., 2015, Martín-Izard et al., 2016). In general, the formation of massive sulfide deposits in the IPB is related to hydrothermal systems where the prevailing modified seawater circulated in the PQG and VSC sequences, having the volcanic centers mostly (but not exclusively) as feeding heat sources (Tornos, 2006). These systems may have focused discharging fluids where metals (mostly Cu, Zn, and Pb) precipitate as sulfides. Usually, the discharged sites correspond to stockwork mineralization, above which the massive sulfides bodies develop. As the result, the host rocks show alteration haloes, a chloritie-dominant proximal alteration zone in the stockwork surrounded by a more distal sericite-rich alteration zone (Barriga 1990; Large et al., 2001; Relvas et al., 2006a,b).

Grounded in metallogenic models, characteristics of the hydrothermal systems, types of associated volcanic rocks and detailed physical volcanology processes, the large size and high density of the massive sulfides, have allowed the successful use of several mineralogical, geochemical, and geophysical methods in the discovery of deposits in the IPB. This success is well documented by the increase in reserves with recent discoveries, such as Aguas Teñidas, Lagoa Salgada, Migollas, Masa Valverde, Vallejín, and Las Cruces (Oliveira et al., 1998; Sáez et al., 1999; Matos et al., 2000; Inverno et al., 2015a; de Oliveira et al, 2011).

The current challenge relies mostly in refining the exploration techniques and models to target deeper and still undiscovered resources. In particular, the VSC sequences of the IPB tend to be at deeper levels towards the W-NW as opposed to the E, where the majority of the deposits have been discovered. The deposits of Neves Corvo and Lagoa Salgada (Leca et al., 1983; Oliveira et al., 1993, 1998; Inverno et al., 2015b) are examples of buried deposits outlined by gravity anomalies, while the Gavião deposit, under the Cenozoic cover, is probably an extension of the Aljustrel system to the NW of the Messejana Fault Zone (Schermerhorn, 1971; Leitão, 1997).

3. Methods

3.1. Sampling and analytical procedures

A total of 4267 stream sediment samples were collected in the 1990's, all over the SPZ, by the Rio Tinto Group under Sociedade Mineira Rio Artezia, thus covering the IPB, PLT, BAFG, and the southern border of the OMZ (Fig. 3). According to the company technical reports, the samples were processed and analyzed at Chemex Labs (Canada) by means of four-acid digestion for ICP-AES and by XRF. Major elements were reported in % and include Al, Ca, Fe, K, Mg, Na, P, S, and Si; analyzed minor elements were Ag, As, B, Ba, Be, Bi, Cd, Co, Cr, Cu, F, Ga, Ge, In, Li, Mn, Mo, Ni, Pb, Rb, Sb, Sc, Se, Sn, Sr, Te, Th, Ti, U, V, W, Zn, and Zr (all reported in ppm), and Au (reported in ppb). The accuracy and precision of the preparation and instrumental performances were checked using 8 international reference samples and 53 duplicates, respectively.

3.2. Concentration-area and singularity mapping

The concentration-area (C-A) method proposed by Cheng et al. (1994) is based in the simple premise that as average concentrations get higher areas enclosing them get smaller following a power law relationship, which can be derived mathematically when grades have a multifractal distribution.

The C-A method procedure is very simple and requires the following steps:

1. Divide the sampled area with a regular grid whose size guaranties that all unit areas within the sample domain boundary has at least one sampled point. For areas enclosing more than one sample, take the average grade for those unit areas;
2. Define a sequence of n grades $\nu_i (i = 1, \cdots, n)$ in ascending order and calculate the cumulative sum of areas enclosing grades $\rho \geq \nu_i$ for each i;
3. Project the results in a log–log plot and adjust a linear model to each of the distinct linear domains of the projected points.

The premise of the C-A model, once at least 2 distinct linear models fit the data, is that a threshold exists if ν_t is the common solution of the equations

$$A(\rho < \nu_t) \propto \rho^{-\alpha_1} \quad (1)$$

and

$$A(\rho \geq \nu_t) \propto \rho^{-\alpha_2} \quad (2)$$

Therefore, ν_t is the threshold separating the set of background grades defined by Eq. (1) from the set of anomalous grades defined by Eq. (2).

These equations also show that a threshold ν_t divides two (or more, if several thresholds define different anomaly levels) linear branches of experimentally calculated areas as a function of enclosed grades in log–log space.

Because the stream sediment data are not regularly spaced the average nearest neighbour was calculated using all points of the sampled space. The calculated average nearest neighbour (aNN) for the SPZ stream sediment data was 795 m, which gives approximately 1.25 samples per km^2. The grid used to cover the sampled space had a spacing equal to $1.2 \times aNN$.

Singularity mapping (Cheng, 2007) uses the concept of singularity, as defined by the singularity exponent of multifractal phenomena, to characterize the anomalous behavior of natural phenomena that can be ascribed to the release of significant amounts of energy concentrated in a relatively small domain.

The singularity index, $\alpha(x)$, for a defined area centered at x, relates the measure (concentration) $\mu(x, \varepsilon)$ at location x with the corresponding area of size ε by the relation

$$\mu(x, \varepsilon) = c\varepsilon^{\alpha(x)}$$

in which both c and $\alpha(x)$ are independent of ε. Applying this concept to geochemical variables requires the use of an average density value, $\langle \rho(x, \varepsilon) \rangle$, as the average measure $\langle \mu(x, \varepsilon) \rangle$ per unit area, ε^E, where E is the Euclidian space dimension (Cheng, 2007), which is to say

$$\langle \rho(x, \varepsilon) \rangle = \frac{\langle \mu(x, \varepsilon) \rangle}{\varepsilon^E} \sim c\varepsilon^{\alpha(x)-E} \quad (3)$$

The singularity, $\alpha(x)$, can be estimated by least squares in log–log space in which the slope equals $\alpha(x) - E$ in the following way:

1. Define a minimum area with size length $\varepsilon_{min} = \varepsilon_1$, that can be set to $1.2 \times aNN$, as previously referred;
2. Define a range $i (i = 1, \cdots, k)$ of areas of linear size $\varepsilon_{min} = \varepsilon_1 < \varepsilon_2 < \cdots < \varepsilon_k = \varepsilon_{max}$, centred at a point x_j, and compute the average density measure $\langle \rho(x, \varepsilon_i) \rangle$ for each area. The maximum area size used was $\varepsilon_{max} = 6 \times aNN$;
3. Compute $\alpha(x)$ form the linearization of Eq. (3) by least squares;
4. Repeat steps 1–3 for each point x_j, $(j = 1, \cdots, N)$, covering the whole sampled space.

The values of $\alpha(x) - E$ computed may have the following outcomes:

- $\alpha(x) < E$ or $\alpha(x) - E < 0$, if and only if $\rho(x, \varepsilon)$ is a decreasing function of ε, meaning that as ε decreases the density increases, and represents an enrichment and a positive singularity;
- $\alpha(x) > E$ or $\alpha(x) - E > 0$, if and only if $\rho(x, \varepsilon)$ is an increasing function of ε, meaning that as ε decreases the density also decreases, and represents a depletion and a negative singularity;
- $\alpha(x) = E$ or $\alpha(x) - E = 0$, if and only if $\rho(x, \varepsilon)$ is constant, independent of size ε, and the measure is simply proportional to the area.

All outputs were processed with ArcGIS software.

4. Results

The geochemical characteristics of the stream sediments are divided into two major domains roughly separated by the Guadiana River which flows towards the South in a general N-S direction (Fig. 4). This main river, marking most of the Portuguese and Spanish border in this region constitutes a hydrological barrier separating stream sediments to the E and W of the main river (Fig. S3 and Table S3). This separation also crudely defines different source areas of the analyzed samples: (i) mostly, the lowermost VSC sequences and extensive PQG exposures to the East in the Spanish part of the SPZ, where numerous massive sulfide deposits occur; and (ii) primarily, the BAFG flysch-type successions, enveloping discontinuous VSC and/or PQG windows (due to diverse structural arrays), to the West. As noted previously, in the Western domain of the SPZ, the volcano-sedimentary sequences potentially hosting the sulfide ore systems are buried deep below BAFG and/or Meso-Cenozoic sediments, which in part justifies the uneven number of known and discovered massive sulfide deposits in the Portuguese sector: just ≈10% of all known deposits in the IPB.

The singularity index data allowed a detailed analysis attributing each of the sampled stream sediments to their main source, i.e. the determinant rock types involved in their composition (Table S3). In this procedure, and because the geochemical signal related to ore systems and their host rocks is stronger to the East of the Guadiana River, all samples picked in this region were grouped and labelled as "IPB Spain". Besides, considering the major aim of the present work, the search for deposits under cover is most significant to the West of that River, i.e. in the Portuguese sector of the SPZ. Using a selected number of elements, average concentrations were estimated for each assortment of rock

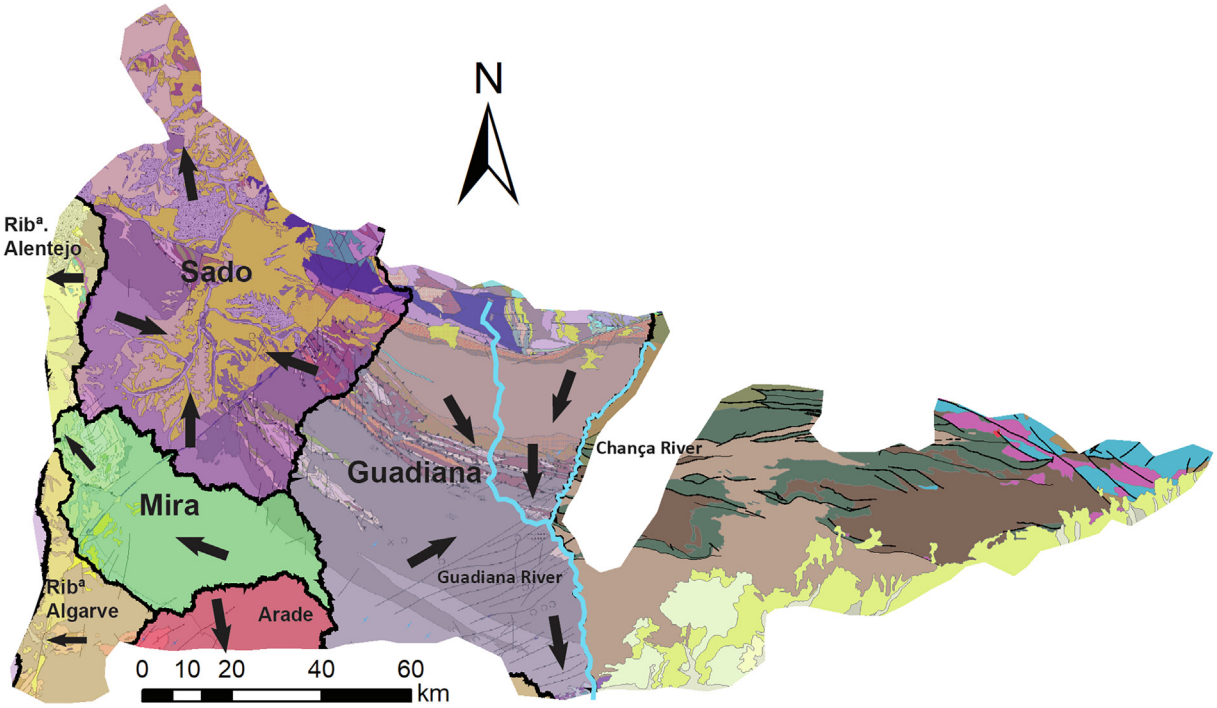

Fig. 4. Delimitation of the hydrographic basins in Portugal, with arrows indicating the general surface flow direction and discharge in the basins. Both, the Guadiana and Chança rivers are indicated; Guadiana river marks the Portuguese-Spanish border from South until half-way up in the map, where the border is marked by the Chança river up until the vicinity of the limit between the SPZ and OMZ. Underlying geological maps are the same as in Fig. 3.

Table 1
Average concentrations of stream sediments for selected elements in the different units and formations of the SPZ.

Units and Formations		Mg	Sc	Sr	Th	U	V	Cu	Zn	Pb	Co	Mn
Pulo do Lobo Terrane		0.55	15.3	99.7	12.5	3.2	148	25.4	68.9	34.4	14.5	885
Phyllite-Quartzite Group		0.53	14.1	79.7	11.7	2.8	126	51.7	118.2	26.0	16.6	1197
Volcanic Sedimentary Complex		0.49	11.8	91.2	17.0	3.9	96	42.9	148.1	76.1	15.5	2163
Flysch Group	Mértola Fm.	0.66	12.0	108.2	8.1	2.9	110	30.5	62.1	218.9	9.4	682
	Mira Fm.	0.55	15.8	87.3	10.8	2.9	152	35.1	89.5	33.2	22.4	1778
	Brejeira Fm.	0.31	13.7	92.0	10.6	3.1	139	29.4	69.1	27.4	33.8	1725
Mesozoic Sedimentary Cover		0.36	7.5	66.2	9.2	2.9	78	23.9	67.1	18.2	12.2	923
IPB Spain		0.78	15.9	28.8	7.7	2.5	137	49.9	94.5	51.8	18.7	1153

Table 2
Maximum concentrations of stream sediments for selected elements in the different units and formations of the SPZ.

Units and Formations		Mg	Sc	Sr	Th	U	V	Cu	Zn	Pb	Co	Mn
Pulo do Lobo Terrane		3.07	47	449	32	7	411	66	142	254	49	3783
Phyllite-Quartzite Group		1.49	47	185	44	6	331	607	1994	2147	32	5194
Volcanic Sedimentary Complex		1.80	51	350	139	19	405	931	2720	28,097	57	42,063
Flysch Group	Mértola Fm.	2.68	52	345	49	7	290	611	635	2087	44	8291
	Mira Fm.	1.37	29	235	57	9	379	111	1708	1145	700	75,701
	Brejeira Fm.	0.89	23	369	18	9	335	95	347	57	223	12,193
Mesozoic Sedimentary Cover		3.40	27	360	110	17	427	2332	6809	2716	124	22,580
IPB Spain		3.81	54	592	52	8	712	1882	4360	3260	169	16,400

types forming the main geological units (PLT, PQG, VCS, BAFG and Meso-Cenozoic covers) and Formations included in BAFG; Table 1 summarizes the results obtained, highlighting the higher concentration for each element. Table 2 shows the maximum concentration obtained for each element in the same geological units or Formations, emphasizing the higher value reached. In this case, values correspond to the maximum absolute concentrations for each element in the data set.

Stream sediments mostly fed by VSC sources display relatively high Th and U values, both average (17.0 and 3.9 ppm respectively) and maximum concentrations (139 and 19 ppm, respectively). The VSC and PQG units also present the highest average values in Cu and Zn, but the highest average concentration for Pb comes from the Mértola Formation (218.9 ppm), belonging to BAFG, followed by the VSC (76.1 ppm) and the "IPB Spain" group (51.8 ppm). The average concentrations in Mn are relatively high in several units, with the highest in the VSC (2163 ppm), but also significant in the BAFG (1778 and 1725 ppm), while the PQG and the "IPB Spain" group have similar average concentrations (1197 and 1153 ppm, respectively). The average concentrations of Co are particularly noteworthy in the Mira Formation from BAFG (22.4 ppm) having a maximum value significantly higher than in the other lithological groups (3 to > 10 times higher). Understanding the meaning of these average concentrations is

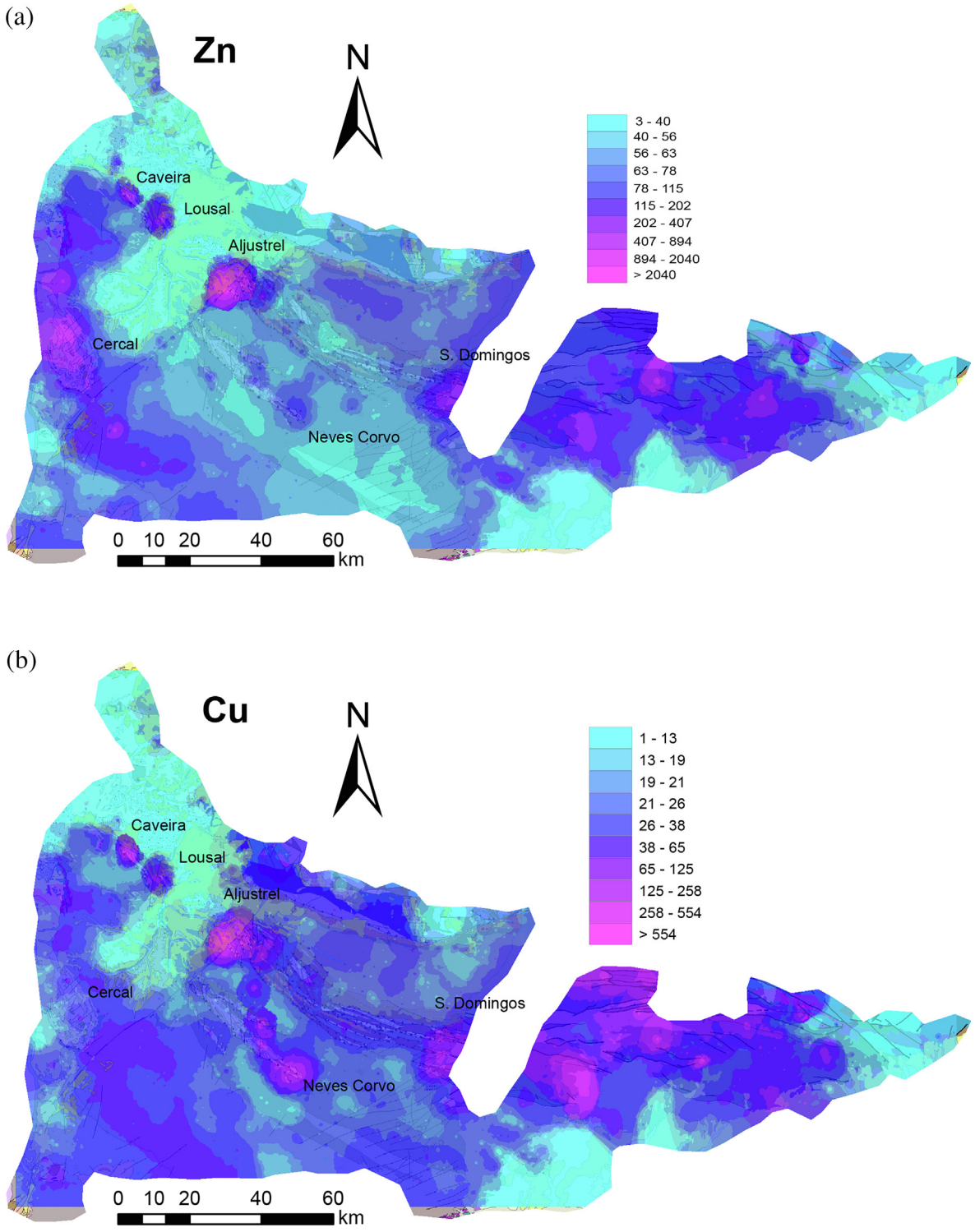

Fig. 5. Geochemical map distribution of Zn (a), Cu (b), Pb (c), and Co (d) in ppm. The observed underlying geological maps are from the 1:500,000 scale geological map of Portugal (LNEG; Fig. S1), and the 1:1,000,000 scale geological map of the Iberian Peninsula (IGME). WMS server links of the maps as in Fig. 3.

not simple; indeed, the analyzed samples include fractions derived from different sources (i.e. various rock types forming the geological substratum subjected to weathering), being also dependent on the geomorphology and surface drainage network; therefore, multiple signals are expected. These aspects will be discussed in the next section, but they are quite useful for the presentation of the maximum concentration for each element (Table 2). The maximum concentrations in the VSC show an atypically high value for Pb (28097 ppm), as compared with the remaining lithological groups and considering Pb distribution in the VSC, which is derived from historical mining residues accumulated at Caveira site (Mateus et al., 2008), followed by 3260 ppm in the "IPB Spain" group. However, the most significant remarks that can be made on the basis of this first inspection of results are: (i) the maximum concentrations of Cu and Zn in the Meso-Cenozoic sedimentary cover; and (ii) the maximum concentrations for Co and Mn in the Mira Formation of BAFG.

Geochemical maps for the elements of interest, such as Cu, Zn, Pb, and Co were produced with IDW and displayed by setting the contour

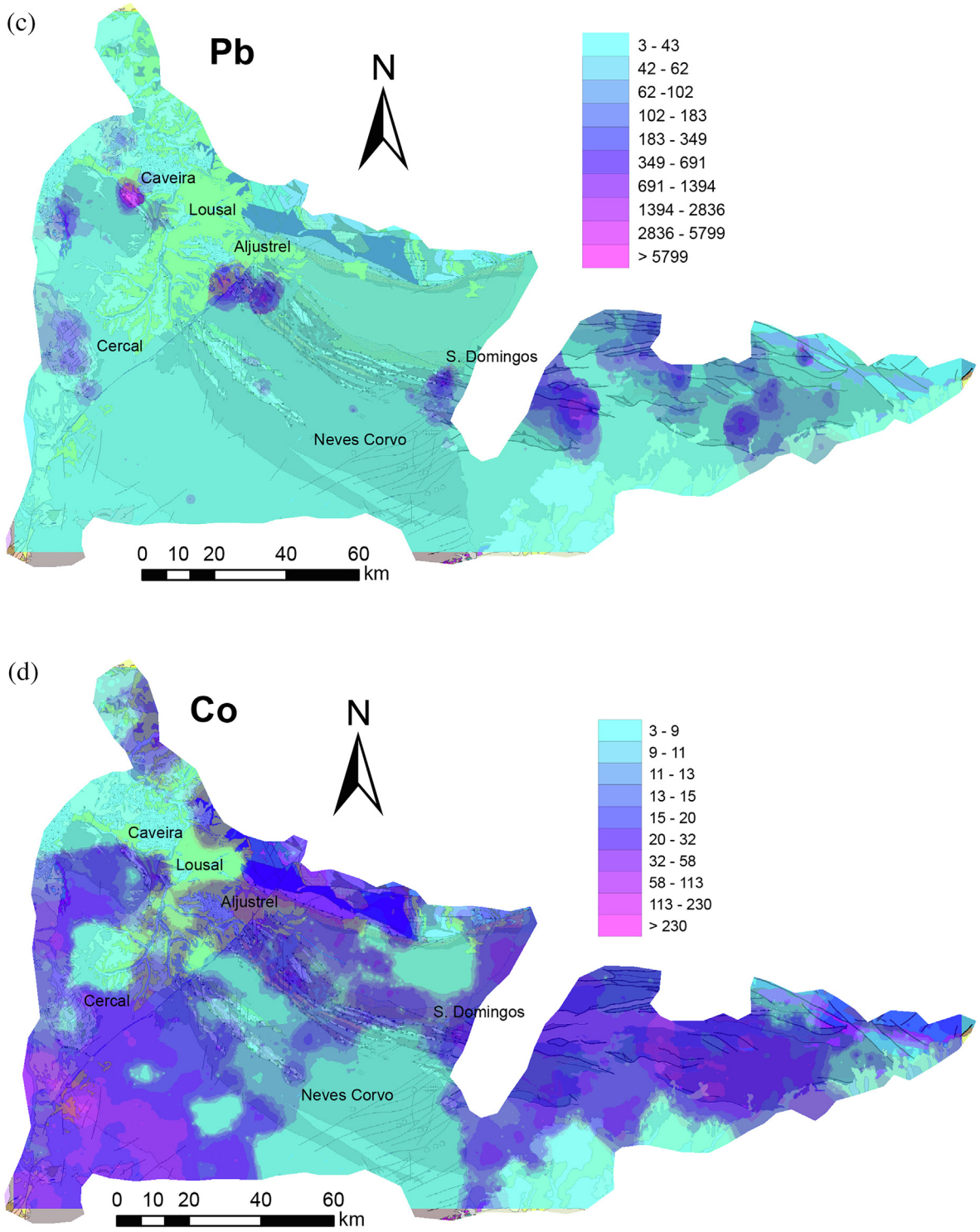

Fig. 5. (*continued*)

classes with the geometric interval algorithm showing the main mineralization areas of IPB (Fig. 5a–d). In all these maps a much higher background is observed towards the East, in the Spanish sector, as outcropping mineralization signs and deposits, and their host rocks (VSC and PQG sequences) are much more regular and continuous. In the Portuguese sector of the IPB, the mapped highest concentration domains overlay also areas where known deposits exist and can be detected by stream sediments due to outcropping, or to accumulations of old and/or modern mining wastes/residues; that is the case of S. Domingos, Aljustrel, Lousal, Caveira, Cercal, and Neves-Corvo (note that the stream sediment survey was performed few years after the exploitation beginning in this giant deposit). These correspondences are particularly evident in Cu and Pb geochemical maps. Zinc shows a more varied distribution, with several domains displaying relatively high contents, especially those supplied by the Mira Formation of BAFG, which are also outlined by the spatial distribution of Cu; this is also particularly relevant considering the distribution of Co (Fig. 5d).

The threshold values obtained with the C-A method for Cu, Zn, Pb, Co, As, and Mn (Table 3) define: (i) regional backgrounds; (ii) local higher backgrounds (2nd threshold) likely related to the main

Table 3
Calculated thresholds with the C-A method.

Element	Threshold #1	Threshold #2	Threshold #3
Cu	20.4	68.0	328.2
Zn	41.7	796.0	3461.6
Pb	16.7	87.6	1105.1
As	9.3	38.8	342.8
Co	16.9	82.9	146.9
Mn	613.2	–	–

outcropping mineralized sites and their host rocks; and (iii) areas enclosing the major deposits (3rd threshold). However, it should be stressed that higher Zn values mostly highlight the Aljustrel mine area. Additionally, for all these base metals considered, the 1st threshold clearly defines the overall regional background. The concentration distribution for manganese displays a simpler structure presenting just one threshold (plots in SI file).

4.1. Anomaly delimitation with singularity mapping

The C-A method has severe limitations for the search of second order patterns related to fainter and less defined anomalies. Indeed, geochemical maps often show a variety of patterns that suggest a much more complex structure which is missed by the C-A method, requiring for a complementary analysis. The maps of the singularity index are shown in Fig. 6 for Cu and Zn. Using the results for the simulation of 5 distinct geochemical map configurations, 10 to 30% of the anomalous areas are still detected with a cut-off set at 70% of the minimum singularity index, considering that the random noise corresponds to the average of 0.7 to 0.8 of the maximum concentration (Table S4 and further explanation in the SI file). Higher background noise, with mean above 0.9 times the highest measured concentration, effectively mask a substantial number of anomalous areas. Considering that the range of the minima of the singularity index in the maps of these simulations is around −0.1, a maximum threshold for the potential identification of faint anomalies can be provided using the multiplying factor of 0.7 as defined in the stochastic simulation of geochemical distributions (see SI file).

There are some features outlined from the singularity map for Zn that differ from what is immediately observed for Cu and Pb; equivalent maps for Co and Mn do not show particular structures. The strongest anomalies in Cu and Pb are related to the main mineralizing systems, especially the domain Aljustrel – Neves Corvo, as well as Caveira and Lousal. For Zn, these features are also observed, although less strongly, but some fainter anomalies related to the westernmost VSC units and over the Mira Formation (BAFG), are clearly noted; these features are also observed in the geochemical map of Zn. Note that the anomaly patterns in the Spanish side of the IPB do not show as clearly the anomalous areas because the continuity of geological exposures of mineralization sites and their host rocks provides a much higher than average background decreasing the contrast with the anomalies which do not stand out as well in the singularity mapping.

These observations apparently do not provide much insight into deep seated deposits. So, the analysis must now turn into the lithological units worth investigation, namely the Mira and Mértola Formations of BAFG and the Meso-Cenozoic sediments to the NW of the Messejana Fault. For that purpose, the minimum singularity exponents characterizing these three geological units were extracted (Table S4) and a threshold with a 0.7 multiplying factor to the minimum value was applied. Using this threshold (Fig. 7a–c) the highest ranked anomalies were marked, most of them sited along the geological contacts with the VCS. So, these anomalies have the same cause as those previously identified and, depending on the unit and element considered, they outline again the known deposits of Aljustrel, Neves-Corvo, S. Domingos, Lousal, and Caveira. The exception is Zn, where a major anomaly to the SE of the VSC anticline of Cercal is clearly noted. However, setting a maximum of −0.1 (Zn and Cu) to −0.2 (Co) for the singularity index based in the simulation analysis, the information becomes more significant. The key aspects to note are the following (Fig. 7a–c):

a) Over the Mira Formation of BAFG (Fig. 7a), an array of combined anomalies for Zn and Co defines a trend that extends up to the Cercal anticline, where the westernmost VSC exposures are known. Minor Cu, Zn, and Co anomalies overlay mapped fault zones, such as the Messejana Fault and several other subsidiary NE-SW structural discontinuities. Some of these minor anomalies are close to the contact between the Mira and Mértola Formations (BAFG) towards the SE and NW of the Messejana Fault.
b) Over the Mértola Formation of BAFG (Fig. 7b) the outlined anomalies farther from the contacts with VSC and PQC units are small-scale and in part related to known NE-SW, fault-controlled, epigenetic ore systems;
c) Over the Meso-Cenozoic sedimentary sequence (Fig. 7c) only Cu and Zn signals are meaningful. Besides the major anomalies identified close to some known deposits (Aljustrel, Caveira, and Lousal), the combined anomalies for Zn and Cu develop a noteworthy trend that includes windows of VSC sequences (close to the OMZ border) and the site below which the deep buried deposit of Lagoa Salgada is located.

Finally, it should be noted that feeble geochemical irregularities over the IPB and PLT are meaningless because the resolution of the data set is insufficient to suitably define faint anomalies over area having very high geochemical backgrounds. Nevertheless, these domains of SPZ remain major targets for exploration of deep buried deposits, some recently targeted for further investigation on the basis of soil geochemical data (Luz et al., 2012, 2014a,b).

5. Discussion

The examined stream sediments geochemical database is the most complete regional catalogue available for the SPZ, therefore covering the IPB throughout its extension. Also, the main features displayed by modern drainage basins in SW Iberia, as well as the meteorological conditions affecting this region, did not promote deeply weathered rocks neither highly dispersed elements from stream sediments, thus making easier relating the multi-element concentrations obtained for stream sediments with their prevalent sources. Nonetheless, this association was done using the 1:500,000 scale geological map (LNEG; http://geoportal.lneg.pt/geoportal/mapas/index.html?servico=CGP500k) and several levels of uncertainty are inherent in this procedure. At this scale, several details are necessarily missed by the geological map that cannot be fully translated to the sample association. Also, the uncertainty of the geological limits may lead to misclassifications of samples close to these limits (that sample location itself is affected by a similar uncertainty). Ideally, this information should have been taken during sample collection, which may not be entirely error-free either. Moreover, these samples also have the additional problem of comprising fractions derived from different (rock/unit) suppliers, especially when originated in sources nearby geological limits. In fact, this note of caution can justify much of the anomalous values above the highest threshold detected over the Mértola and Mira Formations of the BAFG and over the Meso-Cenozoic sedimentary cover, since they mostly occur along the contacts of these formations with the VSC, and near major known and exploited massive sulphide ore deposits. Therefore, the maximum values registered over BAFG formations and Meso-Cenozoic sediments (Table 2) reflect much of the mixing character of the stream sediments fed by source areas that include outcropping mineralized zones and/or (active or historical) mining areas. These maximum values are well above the average concentrations observed in BAFG and Meso-Cenozoic sediments, especially

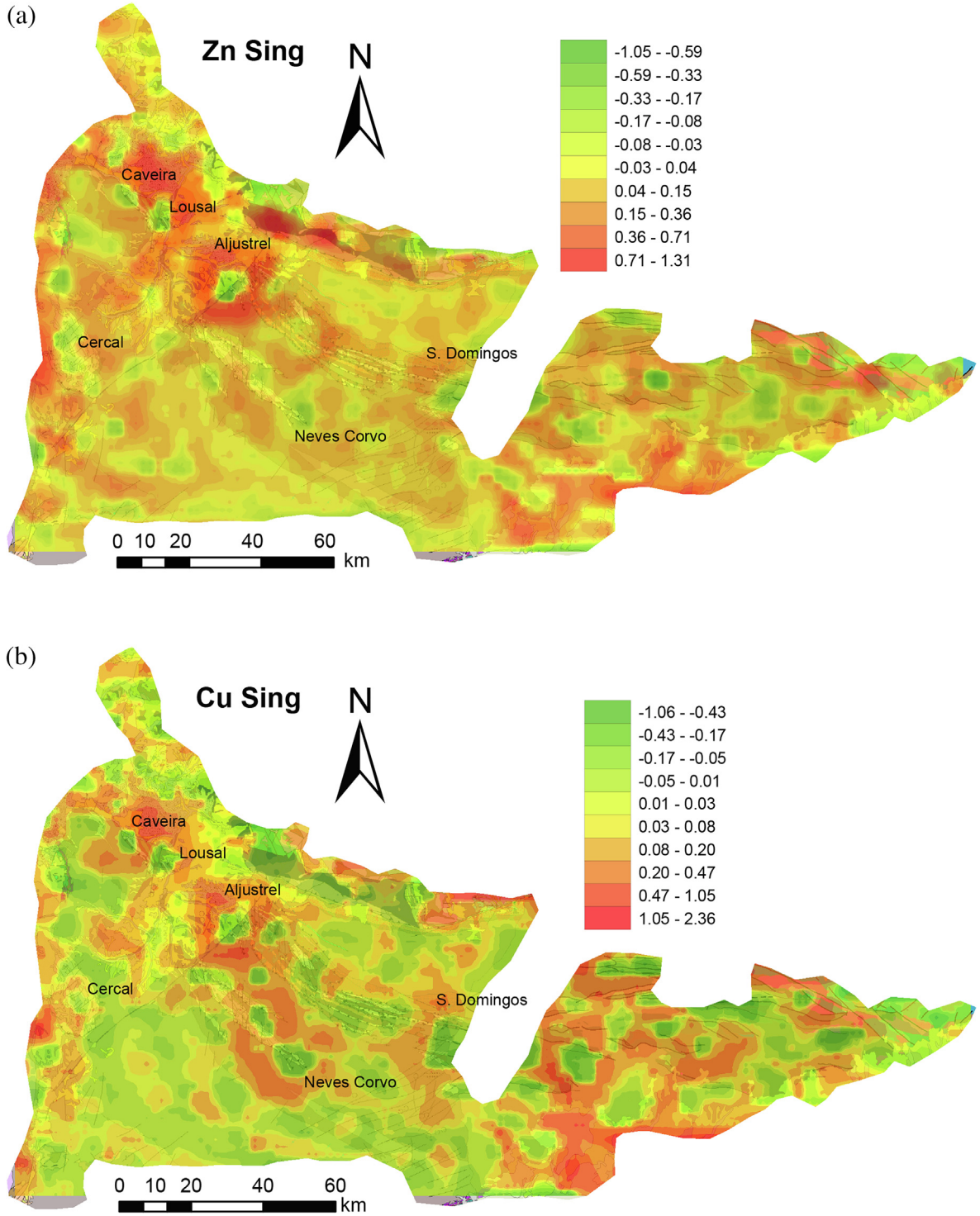

Fig. 6. Singularity index map of Zn (a) and Cu (c). The observed underlying geological maps are the same as in Fig. 3.

if compared with values that typify VSC and PQG sequences. That is particularly evident for Cu, Zn, and even Pb and Mn in Meso-Cenozoic sediments, but also for Zn, Pb, and Mn in the Mira Formation of BAFG; the case for Co is different and will be discussed later. The average values reported are consistent with the data independently gathered (Jorge et al., 2013) for metamorphosed greywackes and shales forming the Mértola, Mira, and Brejeira Formations of BAFG (Tables 4 and 5). Delimitation of the drainage basins (Fig. 4) indicate that mixing sources may be more problematic in the Meso-Cenozoic sediments even though the general flat-lying topography and gentle slopes in the Sado basin do not favour much mixing. On the other hand, a great part of sediments collected over the Mira formation receives very little influence from other source rocks. All these aspects are compatible with the observation that higher grade anomalies are only found in the vicinity of mineralizing systems hosted in VSC sequences. The dispersion character of these anomalies is thus rather weak.

The analysis of the anomalies associated with lower value thresholds, which were listed in the previous section, show a very different picture. In the Mira Formation, the singularity index data of Zn, Co and Cu over Mira Formation show a clear NW-SE trend that extends to the

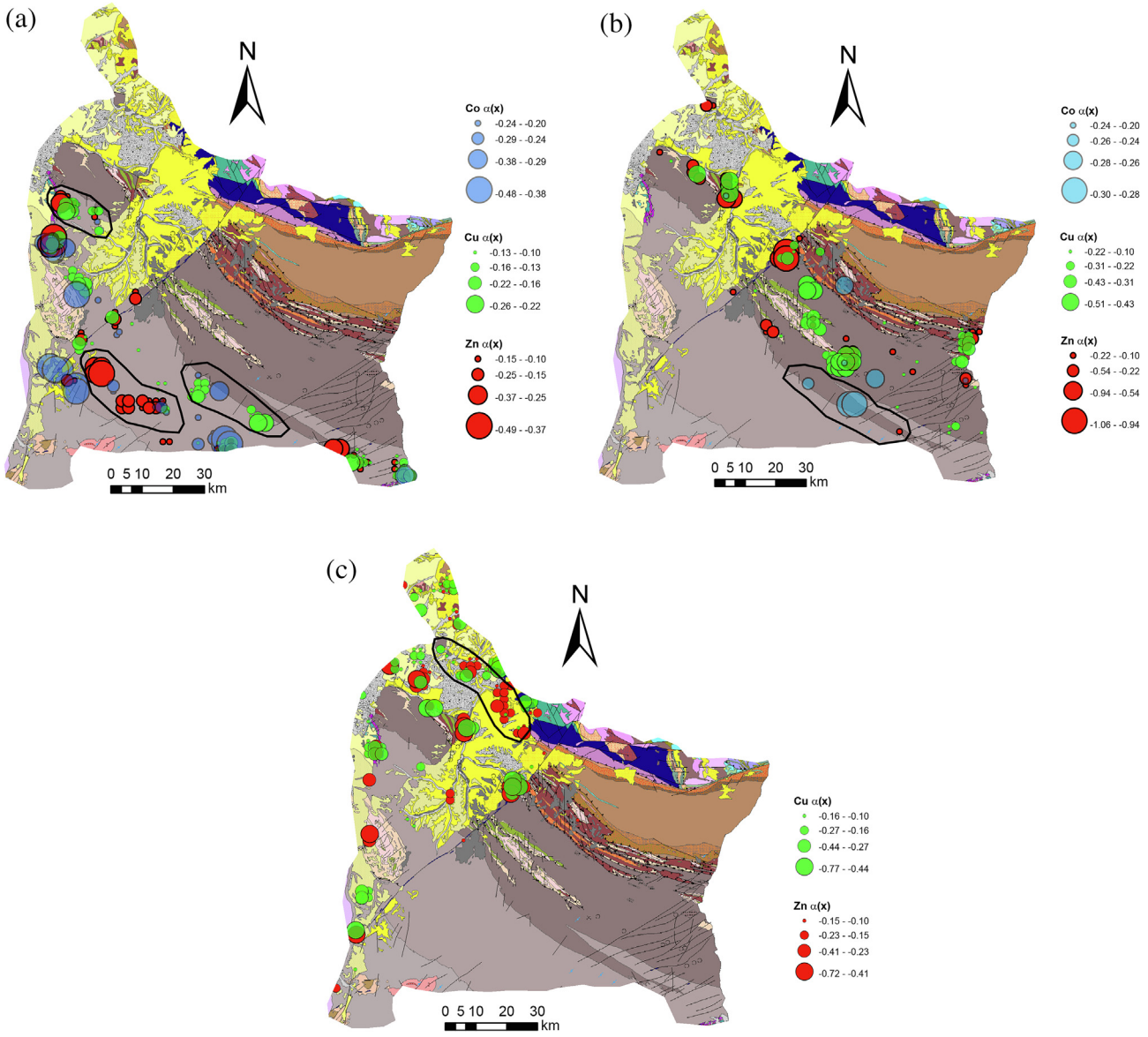

Fig. 7. Extraction of the singularity indexes for Cu, Zn, and Co in the Mira (a) and Mértola (b) Formations, setting maximum values of −0.2 for Cu and Co and −0.1 to Zn. Singularity indexes for Zn and Cu in the Meso-Cenozoic sedimentary cover are shown in (c) with both indexes set at a maximum of −0.1. The polygonal areas refer to the domains with detected faint anomalies whose singularity index is below the defined threshold (discussion in text) for which there is no known geological cause for their existence based on location relative to other lithological formations and active mining sites or detected surface mineralizations in the field.

VSC sequences forming the Cercal anticline to the NW of the Messejana Fault Zone (Fig. 6a; Fig. S1); this anomalous trend is also seen in the geochemical maps of Zn, Co and Cu (Fig. 5). Based on the results with simulated geochemical distributions, the magnitude of the singularity index is equivalent and even higher than the minimum value obtained for anomalous zones overprinted with normally distributed random noise with an average of up to 80% the magnitude of the highest anomalous value. In this area, differences between Zn concentrations may reach nearly 100%, while for Cu and Co they may reach 50%. The trend near the limit between the Mira and Mértola Formations of the BAFG is not seen within the geochemical maps but is suggestive in the singularity maps. This may in part reflect the difference in the background concentration of these elements in Mira and Mértola Formations. Another trend is depicted in the Mira Formation, to the NW of the Messejana Fault (Fig. 7a). This lower grade anomaly is strong in the contact with units of the Triassic (red sandstones) and Lower Jurassic (dolomitic limestones and marls) where signs of Cu carbonate-hosted mineralizations occur. The source of Cu in these mineralized occurrences is unknown and no further studies were undertaken apart from soil geochemistry surveys and general geological reconnaissance of key outcrops. However, this anomaly continues towards the SE for both Cu and Zn generating a general NW-SE trend similar to those viewed in the remaining sectors.

An additional NW-SE trend of lower grade anomalies run over the Cenozoic sediments including the site below which the deep buried deposit of Lagoa Salgada is located (Fig. 7c; Fig. 1). However, these faint anomalies do not emerge in the geochemical map of Cu, and only very slightly in the map of Zn; differences in concentration are enough to depict singularity index values of at least −0.1. The majority of these sediments belongs to the Sado Basin and mostly constitute the result of weathering and physical transport of materials from the Variscan basement whose distribution is mostly controlled by the Messejana Fault Zone, which allowed preserving the sediments in the north-western block. Some of these sediments have extreme high metal concentrations near weathered surface mineral deposits. Nevertheless, the above referred trend of lower grade anomalies depicts also some small

Table 4
Average, maximum, and minimum concentrations for selected elements analysed in the greywacke rocks of the different formations of the BAFG (from Jorge et al., 2013).

Lithology	Greywackes								
	Mértola Fm. (n = 20)			*Mira Fm.* (n = 13)			*Brejeira Fm.* (n = 8)		
Element	*Aver.*	*Max*	*Min*	*Aver.*	*Max*	*Min*	*Aver.*	*Max*	*Min*
Sc	15.4	23.0	11.0	12.4	16.0	8.0	7.6	10.0	6.0
V	122.6	169.0	79.0	94.6	117.0	62.0	62.1	89.0	46.0
Cr	70.0	120.0	40.0	78.5	100.0	50.0	55.0	80.0	40.0
Co	13.8	20.0	7.0	12.8	22.0	7.0	10.6	21.0	1.0
Ni	30.5	50.0	20.0	23.1	40.0	20.0	22.5	30.0	20.0
Cu	27.0	130.0	10.0	10.8	20.0	10.0	16.3	60.0	10.0
Zn	83.0	120.0	50.0	79.2	100.0	50.0	71.3	110.0	30.0
As	8.1	16.0	5.0	7.7	18.0	5.0	31.5	164.0	5.0
Rb	74.5	160.0	44.0	72.0	90.0	57.0	59.1	76.0	48.0
Sr	245.9	345.0	118.0	97.5	194.0	60.0	53.4	72.0	42.0
Y	21.2	31.2	13.8	23.0	28.3	18.0	24.5	28.7	19.4
Nb	8.0	15.4	6.0	9.8	10.8	7.2	10.7	12.4	9.3
Sn	1.3	3.0	0.5	73.3	914.0	2.0	3.3	12.0	1.0
Ba	373.7	503.0	228.0	266.3	336.0	200.0	213.5	302.0	168.0
Pb	15.7	23.0	9.0	8.4	14.0	5.0	42.1	241.0	5.0
Th	9.0	13.5	6.3	9.0	11.6	5.7	7.3	8.2	6.7
U	2.8	3.6	2.2	2.9	3.7	2.1	2.2	2.6	1.7
La	29.1	42.1	22.4	26.4	36.0	18.2	26.9	32.4	22.8
Ce	58.5	78.0	46.7	54.2	74.4	37.2	57.0	66.0	48.7
Nd	24.6	33.0	18.3	23.3	30.8	16.4	24.3	29.3	20.6
Sm	4.8	6.4	3.5	4.7	6.0	3.5	4.9	6.0	4.1

Table 5
Average, maximum, and minimum concentrations for selected elements analysed in the shale rocks of the different formations of the BAFG (from Jorge et al., 2013).

Lithology	Shales								
	Mértola Fm. (n = 15)			*Mira Fm.* (n = 12)			*Brejeira Fm.* (n = 6)		
Element	*Aver.*	*Max*	*Min*	*Aver.*	*Max*	*Min*	*Aver.*	*Max*	*Min*
Sc	22.5	27.0	18.0	24.0	29.0	19.0	23.0	27.0	20.0
V	160.8	197.0	139.0	180.2	224.0	144.0	192.0	215.0	164.0
Cr	84.0	110.0	70.0	119.2	150.0	100.0	130.0	140.0	120.0
Co	18.5	28.0	10.0	13.2	25.0	3.0	16.0	36.0	7.0
Ni	36.7	70.0	20.0	37.5	130.0	20.0	26.7	60.0	20.0
Cu	51.3	70.0	30.0	44.2	60.0	10.0	38.3	60.0	20.0
Zn	111.3	140.0	70.0	103.3	140.0	70.0	131.7	210.0	80.0
As	10.6	20.0	5.0	14.6	27.0	5.0	13.0	25.0	5.0
Rb	151.9	211.0	119.0	196.3	250.0	175.0	224.5	298.0	201.0
Sr	150.1	209.0	77.0	151.7	216.0	110.0	110.7	127.0	80.0
Y	29.6	33.9	26.1	37.2	75.8	29.5	38.7	40.2	37.3
Nb	10.6	12.6	9.5	15.4	17.7	11.7	19.1	20.5	16.8
Sn	1.2	3.0	0.5	3.5	7.0	0.5	4.2	5.0	4.0
Ba	767.7	975.0	557.0	684.7	867.0	520.0	740.2	1226.0	541.0
Pb	20.7	36.0	11.0	13.9	33.0	5.0	19.3	50.0	5.0
Th	12.3	15.0	10.6	14.9	17.0	12.8	16.2	17.8	15.0
U	3.5	4.6	2.9	4.2	5.8	3.2	4.3	5.4	3.9
La	35.8	47.0	32.0	46.3	57.7	37.2	51.6	61.5	46.5
Ce	74.4	87.5	63.9	95.2	119.0	75.1	106.7	128.0	97.3
Nd	31.2	36.0	27.9	41.2	58.1	33.4	44.5	49.0	41.4
Sm	6.1	7.2	5.3	8.4	13.4	6.8	9.1	10.2	8.5

windows of VSC and PQG enclosed in Cenozoic sediments and barely represented in the geological map used as reference (1:500,000 scale); so it is unclear what should be the effective contribution of those Paleozoic portions to the anomalous trend.

Considering that anomalies following NW-SE trends are fairly consistent and that mineralizing systems were not identified in these domains, a plausible mechanism that can explain its occurrence is to consider the fluids assisting the progressing of Variscan thrust faults as the main players in the mobilization and transport of metals (as documented in other IPB sectors, e.g. Marignac et al., 2003; Fig. 2). The geochemical signals outlined by stream sediments could therefore trace source areas in the Paleozoic basement affected by significant metal mobilization during Variscan deformation; and the strongest trend identified is suggestive of deeper VCS rocks in continuity with the Cercal anticline units towards the SE on the opposite side of the Messejana Fault Zone. If so, this area should be surveyed in detail to target possible massive sulfide orebodies at depth. The lower grade anomalies in the Mira Formation are not strong, but the alignment in the northern block of the Messejana Fault is equally encouraging, justifying a closer look in further exploration endeavors. Note however, that the anomalies covering the geological limit between the Mira and Mértola Formations should be considered as indicative, because they might reflect interference from the anomalous spots related to epigenetic mineralization controlled by the NE-SW trending fault zones.

The metal remobilizations triggered by the hydrothermal activity associated with the late NE-SW fault system cannot be dismissed since they represent a series of detected mineralization sites and small-scale deposits; also discrete anomaly spots occur along the Messejana Fault Zone. The lower grade anomalies in the Mértola Formation are sparse and located mostly towards the SE where several of these late NE-SW fault zones are mapped. The mineral deposits database LNEG – SIORMINP (Fig. S4) shows the presence of several Cu-rich lodes controlled by these structural arrays. Copper in these epigenetic and fault-controlled systems has been considered as possible remobilization of deep-seated massive sulfide deposits, but to date this has never been confirmed. Most likely these epigenetic ore-systems result from metal scavenging from nearby sources (mostly of metasedimentary nature), as documented for other Variscan geotectonic units (Mateus, 2001; Mateus and Noronha, 2001; Mateus et al., 2003; Barroso et al., 2003). In this regard, both the Mértola and Mira Formations of BAFG are potential metal sources considering their average geochemical signature. Besides, the Mira Formation seems to have a more significant sandy-derived continental component, which could explain its high radiometric fingerprint in comparison with both the Mértola and Brejeira Formations (Fig. S2). However, it is not possible to explain this radiometric signature based on the geochemistry, using both the stream sediment data and the information reported in Jorge et al. (2013).

Late Variscan metal remobilizations can also suitably explain many of the Co anomalies (Mira and Brejeira Formations have the highest average Co content), some of them developing NE-SW trends as shown in the geochemical map. Therefore, given the geochemical nature of the BAFG Formations, it seems likely they can also be viewed as a source of Co.

6. Conclusion

Multifractal methodologies were applied to stream sediment geochemical data from SPZ. These methods, in particular the singularity mapping, revealed its usefulness in detecting several domains with faint anomalies. It is shown that a careful geological analysis must be undertaken to suitably place in context these data sets otherwise the detected anomalies may have little meaning for exploration purposes. In the IPB, geochemical surveys at this scale may have limited usefulness and it is demonstrated that for the IPB core domains the background in the target metals is so high that fainter anomalies are difficult to detect and, most importantly, validate.

Among the detected anomalies, two main anomalous trends provide future targets for mineral exploration in domains never before considered, both in the Mira Formation of the BAFG: *i*) the trend contiguous to the VSC units of the Cercal anticline towards the SE of the Messejana Fault; and *ii*) the NW-SE trend linking the mineralized zones in the Mesozoic units and along the geological limit between the Mira Formation and the Cenozoic sediments to the NW of the Messejana Fault. The NW-SE anomalous trend, close to the geological limit between the Mira and Mértola Formations (BAFG) besides being less defined and continuous, can at least in part be due to their distinct geochemical background in Cu, Pb, Zn, and Co and also to the previously mentioned Cu-rich epigenetic ore systems. The anomalous trend in the Cenozoic sedimentary cover does not stand out significantly in the singularity mapping, this being easily and fully discernible from natural geochemical fluctuations; nonetheless, it depicts one of the known volcanic axes that hosts the buried Lagoa Salgada deposit to the NW.

Acknowledgments

This work has received the support from Fundação para a Ciência e Tecnologia (FCT) through the grant UID/GEO/50019/2013 (IDL). The Sociedade Mineira Rio Artezia is acknowledged for providing the stream sediment data. Thanks are also due to two anonymous Reviewers for their valuable suggestions and critical comments that helped us to significantly improve the manuscript.

Appendix A. Supplementary data

Supplementary data to this article can be found online at https://doi.org/10.1016/j.oregeorev.2019.103018.

References

Abat, I., Mata, M.P., Nieto, F., Velilla, N., 2001. The phyllosilicates in diagenetic-metamorphic rocks of the South Portuguese Zone, Southwestern Portugal. Can. Mineral. 39, 1571–1589.

Arias, M., Gumiel, P., Martín-Izard, A., 2012. Multifractal analysis of geochemical anomalies: a tool for assessing prospectivity at the SE border of the Ossa Morena Zone, Variscan Massif (Spain). J. Geochem. Explor. 122, 101–112. https://doi.org/10.1016/j.gexplo.2012.08.007.

Arthaud, F., Matte, Ph., 1975. Les décrochements Tardi-Hercyniens du Sud-ouest de l'Europe. Géometrie et essai de reconstitution des conditions de la déformation. Tectonophysics 25, 139–171.

Barriga, F.J.A.S., 1990. Metallogenesis in the Iberian Pyrite Belt. In: Dallmeyer, R.D., Martínez García, E. (Eds.), Pre-Mesozoic Geology of Iberia. Springer, Berlin, Heidelberg, Berlin, pp. 369–379. https://doi.org/10.1007/978-3-642-83980-1_26.

Barriga, F.J.A.S., Fyfe, W.S., 1988. Giant pyritic base metal deposits: the example of Feitais (Aljustrel, Portugal). Chem. Geol. 69, 331–343. https://doi.org/10.1016/0009-2541(88)90044-7.

Barroso, M., Mateus, A., Figueiras, J., Martins, R., Oliveira, V., 2003. Mineralogy and geochemical characteristics of different superimposed mineralisations at the Enfermarias prospect (Moura, Portugal). VI Congresso Nacional de Geologia, Lisboa (Portugal), Ciências da Terra (UNL), Lisboa, n° esp. V, CD-ROM: F9-F12.

Carvalho, D., Goinhas, J., Oliveira, V., Ribeiro, A., 1971. Observações sobre a geologia do Sul de Portugal e consequências metalogenéticas. Est Notas e Trab Serv Fom Min 20, 153–199.

Carvalho, D., Barriga, F.J.A.S., Munhá, J., 1999. Bimodal Siliciclastic systems: The case of the Iberian Pyrite Belt. In: Barrie, C.T., Hannington, M.D. (Eds), Volcanic associated massive sulfide deposits: Processes and examples in modern and ancient settings. Rev Econ. Geol. 8. pp. 375–408.

Carvalho, J.R.S., Relvas, J.M.R.S., Pinto, A.M.M., Frenzel, M., Krause, J., Gutzmer, J., Pacheco, N., Fonseca, R., Santos, S., Caetano, P., Reis, T., Gonçalves, M., 2018. Indium and selenium distribution in the Neves-Corvo deposit, Iberian Pyrite Belt, Portugal. Mineral. Mag. 82 (S1), S5–S41.

Chen, Z., Cheng, Q., Chen, J., Xie, S., 2007. A novel iterative approach for mapping local singularities from geochemical data. Nonlinear Processes Geophys. 14 (3), 317–324. https://doi.org/10.5194/npg-14-317-2007.

Cheng, Q., 2007. Mapping singularities with stream sediment geochemical data for prediction of undiscovered mineral deposits in Gejiu, Yunnan Province, China. Ore Geol. Rev. 32 (1–2), 314–324. https://doi.org/10.1016/j.oregeorev.2006.10.002.

Cheng, Q., Agterberg, F.P., 2009. Singularity analysis of ore-mineral and toxic trace elements in stream sediments. Comput. Geosci. 35 (2), 234–244. https://doi.org/10.1016/j.cageo.2008.02.034.

Cheng, Q., Xu, Y., Grunsky, E., 2000. Integrated spatial and spectrum method for geochemical anomaly separation. Nat. Resour. Res. 9 (1), 43–52. https://doi.org/10.1023/A:1010109829861.

Cheng, Q., Agterberg, F.P., Ballantyne, S.B., 1994. The separation of geochemical anomalies from background by fractal methods. J. Geochem. Explor. 51, 109–130.

Codeço, M.S., Mateus, A., Figueiras, J., Rodrigues, P., Gonçalves, L., 2018. Development of the Ervidel-Roxo and Figueirinha-Albernoa volcanic seuences in the Iberian Pyrite Belt, Portugal: metallogenic and geodynamic implications. Ore Geol. Rev. 98, 80–108.

da Silva, N.V., Mateus, A., Monteiro Santos, F.A., Almeida, E.P., Pous, J., 2007. 3-D electromagnetic imaging of a Paleozoic plate-tectonic boundary segment in SW Iberian Variscides (S Alentejo, Portugal). Tectonophysics 445, 98–115.

de Oliveira, D.P.S., Matos, J.X., Rosa, C.P.J., Rosa, D.R.N., Figueiredo, M.O., Silva, T.P., Guimarães, F., Carvalho, J.R.S., Pinto, A.M.M., Relvas, J.R.M.S., Reiser, F.K.M., 2011. The lagoa salgada orebody, Iberian Pyrite Belt, Portugal. Econ. Geol. 100, 1111–1128.

Dias, R., Ribeiro, A., 1995. The Ibero-Armorican arc: a collisional effect against an irregular continent. Tectonophysics 246, 113–128.

Dias, R., Moreira, N., Ribeiro, A., Basile, C., 2017. Late Variscan deformation in the Iberian Peninsula; a late feature in the Laurentia-Gondwana dextral collision. Int. J. Earth Sci. (Geol Rundsch) 106, 549–567.

Feliciano, R., Mateus, A., Matos, J.X., 2008. Spatial distributions of Cu, Zn, Pb and Co contents in stream sediments of the South Portuguese Zone; implications for mineral exploration. V Seminario Recursos Geologicos, Ambiente e Ordenamento do Territorio Vila Real 10.

Figueiras, J., Mateus, A., Gonçalves, M.A., Waerenborgh, J.C., Fonseca, P., 2002. Geodynamical evolution of the South Variscan Iberian Suture as recorded by mineral transformations. Geodin. Acta 15, 45–61.

Fonseca, P.E., Ribeiro, A., 1993. The Tectonics of Beja-Acebuches Ophiolite: a major suture in the Iberian Variscan Fold Belt. Geol. Rundsch. 3–82, 440–447.

Fonseca, P., Munhá, J., Pedro, J., Rosas, F., Moita, P., Araújo, A., Leal, N., 1999. Variscan ophiolites and high pressure metamorphism in Southern Ibéria. Ofioliti 24, 259–268.

Fortier, S.M., Thomas, C.L., McCullough, E.A., Tolcin, A.C., 2018. Global trends in mineral commodities for advanced technologies. Nat. Resour. Res. 27, 191–200.

Gonçalves, M.A., Mateus, A., Oliveira, V., 2001. Geochemical anomaly separation by multifractal modelling. J. Geochem. Explor. 72, 91–114.
Gonçalves, M.A., Mateus, A., Pinto, F., Vieira, R., 2018. Using multifractal modelling, singularity mapping, and geochemical indexes for targeting buried mineralization: application to the W-Sn Panasqueira ore-system. Portugal. J. Geochem. Explor. 189, 42–53.
Grunsky, E.C., 2010. The interpretation of geochemical survey data. Geochem.: Explor. Environ. Anal. 10, 27–74.
Hagemann, S.G., Lisitsin, V.A., Huston, D.L., 2016. Mineral system analysis: Quo vadis. Ore Geol. Rev. 76, 504–522.
Humphreys, D., 2013. Long-run availability of mineral commodities. Mineral Econ. 26, 1–11.
Huston, D.L., Mernagh, T.P., Hagemann, S.G., Doublier, M.P., Fiorentini, M., Champion, D.C., Jaques, A.L., Czarnota, K., Cayley, R., Skirrow, R., Bastrakov, E., 2016. Tectono-metallogenic systems – The place of mineral systems within tectonic evolution, with an emphasis on Australian examples. Ore Geol. Rev. 76, 168–210.
Inverno, C., Díez-Montes, A., Rosa, C., García-Crespo, J., Matos, J., García-Lobón, J.L., Carvalho, J., Bellido, F., Castello-Branco, J.M., Ayala, C., Batista, M.J., Rubio, F., Granado, I., Tornos, F., Oliveira, J.T., Rey, C., Araújo, V., Sánchez-García, T., Pereira, Z., Represas, P., Solá, A.R., Sousa, P., 2015a. Introduction and geological setting of the Iberian Pyrite Belt. In: Weihed, P. (Ed.), 3D, 4D and Predictive Modelling of Major Mineral Belts in Europe, Mineral Resource Reviews. Springer, Switzerland, pp. 191–208. https://doi.org/10.1007/978-3-319-17428-0_9.
Inverno, C., Rosa, C., Matos, J., Carvalho, J., Castello-Branco, J.M., Batista, M.J., Granado, I., Oliveira, J.T., Araújo, V., Pereira, Z., Represas, P., Solá, A.R., Sousa, P., 2015b. Modelling of the Neves Corvo área. In: Weihed, P. (Ed.), 3D, 4D and Predictive Modelling of Major Mineral Belts in Europe, Mineral Resource Reviews. Springer, Switzerland, pp. 231–261. https://doi.org/10.1007/978-3-319-17428-0_9.
Jesus, A.P., Mateus, A., Gonçalves, M.A., Munhá, J., 2013. Multi-fractal modelling and spatial Cu-soil anomaly analysis along the southern border of the Iberian Terrane in Portugal. J. Geochem. Explor. 126–127, 23–44.
Jesus, A.P., Munhá, J., Mateus, A., Tassinari, C., Nutman, A., 2007. The Beja layered gabbroic sequence (Ossa-Morena Zone, Southern Portugal): gochronology and geodynamic implications. Geodin. Acta 20, 139–157. https://doi.org/10.3166/ga.20.
Jorge, R.C.G.S., Fernandes, P., Rodrigues, B., Pereira, Z., Oliveira, J.T., 2013. Geochemistry and provenance of the Carboniferous Baixo Alentejo Flysch Group, South Portuguese Zone. Sediment. Geol. 284–285, 133–148. https://doi.org/10.1016/j.sedgeo.2012.12.005.
Large, R., Gemmell, B., Paulick, H., Huston, D., 2001. The alteration box plot: a simple approach to understanding the relationship between alteration mineralogy and lithogeochemistry associated with volcanic-hosted massive sulfide deposits. Econ. Geol. 96, 957–971. https://doi.org/10.2113/gsecongeo.96.5.957.
Lazwcka, P., 2014. Giant metallic deposits – a century of progress. Ore Geol. Rev. 62, 259–314.
Leca, X., Ribeiro, A., Oliveira, J.T., Silva, J.B., Albouy, L., Carvalho, D., Merino, F., 1983. Cadre Géologique des Mineralisations de Neves Corvo (Baixo Alentejo, Portugal). Lithostratigraphie, Paléologéographie et Tectonique. Mémoire Bureau de Recherches Géologiques et Minières 121, 79 pp.
Leistel, J.M., Bonijoly, D., Braux, C., Freyssinet, P., Kosakevitch, A., Leca, X., Lescuyer, J.L., Marcoux, E., Milési, J.P., Piantone, P., Sobol, F., Tegyey, M., Thiéblemont, D., Viallefond, L., 1994. The massive sulphide deposits of the South Iberian Pyrite Province: geological setting and exploration criteria. BRGM Doc. 234, 236.
Leistel, J.M., Marcoux, E., Thiéblemont, D., Quesada, C., Sánchez, A., Ruiz de Almodóvar, G., Pascual, E., Sáez, R., 1998. The volcanic-hosted massive sulfide deposits of the Iberian Pyrite Belt. Miner. Deposita 33, 2–30. https://doi.org/10.1007/s001260050130.
Leitão, J. 1997. Geology of the Aljustrel massive sulfide deposits. Society of Economic Geologists Field Trip Guidebook Series, 27. pp. 82–97.
Li, C., Ma, T., Shi, J., 2003. Application of a fractal method relating concentrations and distances for separation of geochemical anomalies from background. J. Geochem. Explor. 77 (2–3), 167–175. https://doi.org/10.1016/S0375-6742(02)00276-5.
Liu, Y., Zhou, K., Cheng, Q., 2017. A new method for geochemical anomaly separation based on the distribution patterns of singularity indices. Comput. Geosci 105, 139–147. https://doi.org/10.1016/j.cageo.2017.05.008.
Luz, F., Mateus, A., Matos, J.X., Gonçalves, M.A., 2012. Geochemistry of stream sediments southwards of the SW Variscan suture in Portugal (Guadiana and Chança river basins): insights into element anomalies of variable origin and intensity. Appl. Earth Sci. 121, 137–150.
Luz, F., Mateus, A., Matos, J.X., Gonçalves, M.A., 2014a. Cu- and Zn-soil anomalies in the NE border of the South Portuguese zone (Iberian Variscides, Portugal) identified by multifractal and geostatistical analyses. Nat. Resour. Res. 23, 195–215.
Luz, F., Mateus, A., Matos, J.X., Gonçalves, M.A., 2014b. Cu, Zn and Pb soil geochemistry data from the NE domain of the Iberian Pyrite Belt in Portugal; implications to mineral exploration. Geochem. Explor. Environ. Anal. 14, 331–340.
Matte, P., Ribeiro, A., 1975. Forme et orientation de l'ellipsoid de déformation dans la virgation hercynienne de Galice. Relations avec le plissement et hypotéses sur la génese de l'arc ibéro-armoricain. C.R. Academie Sciences Paris, pp. 2825–2828.
Marignac, C., Diagana, B., Cathelineau, M., Boiron, M.-C., Banks, D., Fourcade, S., Vallance, J., 2003. Remobilisation of base metals and gold by Variscan metamorphic fluids in the south Iberian pyrite belt: evidence from the Tharsis VMS deposit. Chem. Geol. 194, 143–165. https://doi.org/10.1016/S0009-2541(02)00275-9.
Marques, F.O., Mateus, A., Tassinari, C., 2002. The Late-Variscan fault network in Central-Northern Portugal: a re-evaluation. Tectonophysics 359, 255–270.
Martín-Izard, A., Arias, D., Arias, M., Gumiel, P., Sanderson, D.J., Castañon, C., Lavandeira, A., Sanchez, J., 2015. A new 3D geological model and interpretation of structural evolution of the world-class Rio Tinto VMS deposit, Iberian Pyrite Belt (Spain). Ore Geol. Rev. 71, 457–476.
Martín-Izard, A., Arias, D., Arias, M., Gumiel, P., Sanderson, D.J., Castañon, C., Sanchez, J., 2016. Ore deposit types and tectonic evolution of the Iberian Pyrite Belt: from transtensional basins and magmatism to transpression and inversion tectonics. Ore Geol. Rev. 79, 254–267. https://doi.org/10.1016/j.oregeorev.2016.05.011.
Mason, L., Prior, T., Mudd, G., Giurco, D., 2011. Availability, addiction and alternatives: three criteria for assessing the impact of peak minerals on society. J. Cleaner Prod. 19, 958–966.
Mateus, A., Figueiras, J., Gonçalves, M.A., Fonseca, P., 1999. Evolving fluid circulation within the Beja-Acebuches Variscan Ophiolite Complex (SE Portugal). Ofioliti 24/2 Sp. Iss. pp. 269–282.
Mateus, A., Figueiras, J., Matos, J.X., Gonçalves, M.A., Lopes, R., Labaredas, J., Beleque, A., 2008. Condicionantes impostas à dispersão de metais acumulados em escombreiras mineiras; o exemplo de Caveira (Faixa Piritosa Ibérica). "A Terra – Conflitos e Ordem", Livro de Homenagem ao Professor António Ferreira Soares, pp. 373–382.
Mateus, A., Matos, J.X., Rosa, C., Oliveira, V., 2003. Cu-ores in quartz-carbonate veins at Estremoz-Alandroal and Barrancos-Sto Aleixo regions (Ossa Morena Zone): a result of Late-Variscan hydrothermal activity. VI Congresso Nacional de Geologia, Lisboa (Portugal), Ciências da Terra (UNL), Lisboa, n° esp. V, CD-ROM: F90-F93.
Mateus, A., Noronha, F., 2001. Late-Variscan crustal uplift of the Iberian Terrane as a response to isostatic rebound; implications for the brittle-ductile transition, fluid circulation and metallogenesis. XVI European Current Research on Fluid Inclusions. Universidade do Porto, Fa-culdade de Ciências, Porto (Portugal), Mem 7, Noronha, F., Dória, A., Guedes, A., (Eds.). pp. 295–298.
Mateus, A., 2001. Dinâmica de fluidos tardi-Varisca; constrangimentos geodinâmicos e implicações metalogenéticas. 7ª Conferência Nacional do Grupo de Geologia Estrutural e Tectónica, Lisboa, Portugal. pp. 12–18.
Matos, J.X., Barriga, F.J.A.S., Oliveira, V.M.J., Relvas, J.M.R.S., Conceição, P., 2000. The structure and hydrothermal alteration of the Lagoa Salgada orebody (Iberian Pyrite Belt – Sado Tertiary Basin). Volcanic Environments and Massive Sulfide Deposits – SEG/-CODES International Conference Abstracts Volume, Tasmania, Australia. pp 119–121.
McCuaig, T.C., Beresford, S., Hronsky, J., 2010. Translating the mineral systems approach into an effective exploration targeting system. Ore Geol. Rev. 38, 128–138.
McCuaig, T.C., Hronsky, J.M.A., 2014. The mineral system concept: the key to exploration targeting. Soc. Econ. Geol. Spec. Publ. 18, 153–176.
Mitjavilla, J., Marti, J., Soriano, C., 1997. Magmatic evolution and tectonic setting of the Iberian Pyrite Belt volcanism. J. Petrol. 38, 727–755. https://doi.org/10.1093/petrology/38.6.727.
Moran, C.J., Lodhie, S., Kunz, N.C., Huisingh, D., 2014. Sustainability in mining, minerals and energy: new processes, pathways and human interactions for a cautiously optimistic future. J. Cleaner Prod. 84, 1–5.
Munhá, J., 1979. Blue amphiboles, metamorphic regime and plate tectonic modelling in the iberian pyrite belt. Contrib. Miner. Petrol. 69, 279–289. https://doi.org/10.1007/BF00372330.
Munhá, J., 1981. Igneous and Metamorphic Petrology of the Iberian Pyrite Belt Volcanic Rocks. Doctoral Thesis. University of Western, Ontario, Canada.
Munhá, J., 1983a. Hercynian magmatism in the Iberian Pyrite Belt. In: Sousa, M.J.L., Oliveira, J.T. (Eds.), The Carboniferous of Portugal. Memórias Serviços Geológicos de Portugal, pp. 39–81.
Munhá, J., 1983. Low-grade regional metamorphism in the Iberian Pyrite Belt. Comun. Serv. Geol. Port. 69, 3–36.
Munhá, J., 1990. Metamorphic evolution of the South Portuguese/Pulo do Lobo Zone. In: Dallmeyer, R.D., Martínez García, E. (Eds.), Pre-Mesozoic Geology of Iberia. Springer Berlin Heidelberg, Berlin, pp. 363–369. https://doi.org/10.1007/978-3-642-83980-1_25.
Munhá, J., Kerrich, R., 1980. Seawater basalt interaction in spilites from the Iberian Pyrite Belt. Contrib. Miner. Petrol. 73, 191–200. https://doi.org/10.1007/BF00371394.
Oliveira, J.T., Horn, M., Kullmann, J., Paproth, E., 1985. The stratigraphy of the Upper Devonian and Carboniferous sediments of Southwest Portugal. C.R. 10e, International Congress Stratigraphy Geology Carboniferous, Madrid, 1. pp. 1–17.
Oliveira, J.T., Horn, M., Paproth, E., 1979. Preliminary note on the stratigraphy of the Baixo-Alentejo Flysch Group, Carboniferous of Portugal, and on the palaeogeographic development compared to corresponding units in NorthWest Germany. Comunicações dos Serviços Geológicos de Portugal 65, 151–168.
Oliveira, V., Matos, J., Bengala, J., Silva, M., Sousa, P., Torres, L., 1993. Lagoa Salgada um novo depósito na F.P.I., Bacia Terciária do Sado. Est. Not. Trab. Inst. Geol. Min. 35, 55–89.
Oliveira, J.T., 1990. In: Stratigraphy and syn-Sedimentary Tectonism in the South Portuguese Zone. Pre-Mesozoic Geology of Iberia, pp. 334–347.
Oliveira, J.T., Pereira, Z., Rosa, C., Rosa, D., Matos, J., 2005. Recent advances in the study of the stratigraphy and the magmatism of the Iberian Pyrite Belt, Portugal. In: Carosi, R., Dias, R., Iacopini, D., Rosenbaum, G., (Eds.). The southern Variscan belt, Journal of the Virtual Explorer, Electronic Edition 19/9. pp. 1441–8142.
Oliveira, J.T., Relvas, J., Pereira, Z., Matos, J., Rosa, C., Rosa, D., Munhá, J., Fernandes, P., Jorge, R., Pinto, A., 2013. Geologia Sul Portuguesa, com ênfase na estratigrafia, vulcanologia física, geoquímica e mineralizações da faixa pitritosa. In: Dias, R., Araújo, A., Terrinha, P., Kullberg, J.C. (Eds.), Geologia de Portugal, Volume 1, Escolar Editora, pp. 673–765.
Oliveira, V., Matos, J.X., Bengala, M., Silva, N., Sousa, P., Torres, L., 1998. Geology and geophysics as successful tools in the discovery of the Lagoa Salgada orebody (Sado Tertiary Basin – Iberian Pyrite Belt), Grândola, Portugal. Miner. Deposita 33, 170–187. https://doi.org/10.1007/s001260050139.
Pereira, Z., 1999. Palinoestratigrafia do Sector Sudoeste da Zona Sul Portuguesa. Comunicações Instituto Geológico e Mineiro, Portugal, pp. 25–57.

Pereira, Z., Matos, J., Fernandes, P., Oliveira, J.T., 2007. Devonian and Carboniferous palynostratigraphy of the South Portuguese Zone, Portugal – An overview. Comunicações Geológicas 94, 53–79.
Pereira, Z., Matos, J.X., Fernandes, P., Jorge, R.G.S., Oliveira, J.T., 2018. Stratigraphy of the Northern Pulo do Lobo Domain, SW Iberia Variscides: a palynological contribution. Geobios. https://doi.org/10.1016/j.geobios.2018.04.001.
Pinto, Á.M.M., Relvas, J.M.R.S., Carvalho, J.R.S., Liu, Y., 2014. High-tech metals in the zinc-rich massive ores of the Neves Corvo Deposit. Comunicações Geológicas 1010, 825–828.
Quesada, C., 1991. Geological constraints on the Paleozoic tectonic evolution of tectonostratigraphic terranes in the Iberian massif. Tectonophysics 185, 225–245.
Quesada, C., Fonseca, P., Munhá, J., Oliveira, J., Ribeiro, A., 1994. The Beja-Acebuches Ophiolite (Southern Iberia Variscan fold belt): geological characterization and geodynamic significance. Boletin Geológico y Minero 105–1, 3–49.
Quesada, C., 1998. A reappraisal of the structure of the Spanish segment of the Iberian Pyrite Belt. Miner. Deposita 33, 31–44. https://doi.org/10.1007/s001260050131.
Rantitsch, G., 2001. The fractal properties of geochemical landscapes as an indicator of weathering and transport processes within the Eastern Alps. J. Geochem. Explor. 73, 27–42.
Relvas, J.M.R.S., Barriga, F.J.A.S., Pinto, A., Ferreira, A., Pacheco, N., Noiva, P., Barriga, G., Baptista, R., Carvalho, D., Oliveira, V., Munhá, J., Hutchinson, R.W., 2002. The Neves-Corvo deposit, Iberian Pyrite Belt, Portugal: Impacts and future, 25 years after the discovery. In: Goldfarb, R., Nielsen, J. (Eds.), Integrated Methods for discovery. SEG Special Publication, pp. 155–176.
Relvas, J.M.R.S., Barriga, F.J.A.S., Ferreira, A., Noiva, P.C., Pacheco, N., Barriga, G., 2006a. Hydrothermal alteration and mineralization in the Neves-Corvo volcanichosted massive sulfide deposit, Portugal: I. Geology, mineralogy, and geochemistry. Econ. Geol. 101, 791–804. https://doi.org/10.2113/gsecongeo.101.4.753.
Relvas, J.M.R.S., Barriga, F.J.A.S., Longstaffe, F.J., 2006b. Hydrothermal alteration and mineralization in the Neves-Corvo volcanic-hosted massive sulfide deposit, Portugal: II. Oxygen, hydrogen, and carbon isotopes. Econ. Geol. 101, 753–790. https://doi.org/10.2113/gsecongeo.101.4.791.
Ribeiro, A., Oliveira, J., Silva, J., 1983. La estructura de la Zona Sur Portuguesa. In: Comba, J.A. (Ed.), Geologia de Espana. Instituto Geológico Mineiro de Espana, Madrid, pp. 504–511.
Ribeiro, A., Quesada, C., Dallmeyer, R.D., 1990a. Geodynamic evolution of the Iberian Massif. In: Dallmeyer, R.D., Martínez García, E. (Eds.), Pre-Mesozoic Geology of Iberia. Springer, Berlin, Heidelberg, Berlin, pp. 334–347. https://doi.org/10.1007/978-3-642-83980-1_28.
Ribeiro, A., Kullberg, M.C., Kullberg, J.C., Manuppella, G., Phipps, S., 1990b. A review of Alpine Tectonics in Portugal: foreland detachment in basement at cover rocks. Tectonophysics 189, 357–366.
Ribeiro, A., Munhá, J., Dias, D., Mateus, A., Pereira, E., Ribeiro, L., Fonseca, P., Araújo, A., Oliveira, J.T., Romão, J., Chaminé, H., Coke, C., Pedro, J., 2007. Geodynamic evolution of the SW Europe Variscides. Tectonics 26, TC6009. https://doi.org/10.1029/2006TC002058.
Ribeiro, A., Munhá, J., Fonseca, P.E., Araújo, A., Pedro, J.C., Mateus, A., Tassinari, C., Machado, G., Jesus, A.P., 2010. Variscan ophiolite belts in the Ossa-Morena Zone (Southwest Iberia): geological characterization and geodynamic significance. Gondwana Res. 17, 408–421. https://doi.org/10.1016/j.gr.2009.09.005.
Rodrigues, B., Chew, D.M., Jorge, R.C.G.S., Fernandes, P., Veiga-Pires, C., Oliveira, J.T., 2015. Detrital zircon geochronology of the Carboniferous Baixo Alentejo Flysch Group (South Portugal); constraints on the provenance and geodynamic evolution of the South Portuguese Zone. J. Geol. Soc. 172, 294–308. https://doi.org/10.1144/jgs2013-084.
Rosa, C.J.P., McPhie, J., Relvas, J.M.R.S., Pereira, Z., Oliveiras, T., Pacheco, N., 2008. Volcanic facies architecture hosting the Neves Corvo VHMS deposit, Iberian Pyrite Belt, Portugal. Miner. Deposita 43, 449–466.
Rosa, C.J.P., McPhie, J., Relvas, J.M.R.S., 2009. The felsic volcanic centres of neves corvo and lousal massive sulfide deposits in the iberian pyrite belt. In: Williams, P.J. (Ed.), Smart Science for Exploration and Mining. Published by Economic Geology Research Unit, James Cook University, Townsville, Australia, pp. 484–486.
Rosa, C.J.P., McPhie, J., Relvas, J., 2010. Type of volcanoes hosting the massive sulphide deposits of the Iberian Pyrite Belt. J. Volcanol. Geoth. Res. 194, 107–126. https://doi.org/10.1016/j.jvolgeores.2010.05.005.
Rosa, D., Inverno, C., Oliveira, V., Rosa, C., 2004. Geochemistry of volcanic rocks, Albernoa area, Iberian Pyrite Belt, Portugal. Int. Geol. Rev. 46, 366–383. https://doi.org/10.2747/0020-6814.46.4.366.
Rosa, D., Inverno, C., Oliveira, V., Rosa, C., 2006. Geochemistry and geothermometry of volcanic rocks from Serra Branca, Iberian Pyrite Belt, Portugal. Gondwana Res. 10, 328–339. https://doi.org/10.1016/j.gr.2006.03.008.
Routhier, P., Aye, F., Boyer, C., Lecolle, M., Picot, P., Roger, G., 1980. La ceinture sud-iberique à amas sulfurés dans sa partie espagnole mediane, tableau geologique et metalogenique, synthèse sur le type amas sulfurés volcano-sedimentaires. Mémoires Bureau de Recherches Geólogiques et Minières 94, 1–265.
Sadeghi, B., Madani, N., Carranza, E.J.M., 2015. Combination of geostatistical simulation and fractal modeling for mineral resource classification. J. Geochem. Explor. 149, 59–73. https://doi.org/10.1016/j.gexplo.2014.11.007.
Sáez, R., Almodóvar, G.R., Pascual, E., 1996. Geological constraints on massive sulfide genesis in the Iberian Pyrite Belt. Ore Geol. Rev. 11, 429–451. https://doi.org/10.1016/S0169-1368(96)00012-1.
Sáez, R., Pascual, E., Toscano, M., Almodóvar, G.R., 1999. The Iberian type of volcano-sedimentary massive sulfide deposits. Miner. Deposita 34, 549–570. https://doi.org/10.1007/s001260050220.
Schermerhorn, L.J.G., 1971. An outline stratigraphy of the Iberian Pyrite Belt. Boletin Geológico y Minero 82 (3/4), 239–268.
Serranti, S., Ferrini, V., Masi, U., Cabri, L.J., 2002. Trace-element distribution in cassiterite and sulfides from rubané and massive ores of the Corvo deposit, Portugal. Can. Mineral. 40, 815–835.
Silva, J., Oliveira, J., Ribeiro, A., 1990. South Portuguese Zone. Structural outline. In: Dallmeyer, R.D., Martinez Garcia, E., (Eds.), Pre-Mesozoic Geology of Iberia. pp. 348–362.
Silva, P., Henry, B., Marques, F.O., Font, E., Mateus, A., Vegas, R., Miranda, J.M., Palomillo, R., Palencia-Ortas, A., 2008. Magma flow, exsolution processes and rock metasomatism in the Great Messejana-Plasencia Dyke (Iberian Península). Geophys. J. Int. 175, 806–824.
Thiéblemont, D., Pascual, E., Stein, G., 1998. Magmatism in the Iberian Pyrite Belt: petrological constraints on a metallogenetic model. Miner. Deposita 33, 98–110. https://doi.org/10.1007/s001260050135.
Tornos, F., Delgado, A., Casquet, C., Galindo, C., 2000a. 300 Million years of episodic hydrothermal activity: stable isotope evidence from hydrothermal rocks of the eastern Iberian Central System. Miner. Deposita 35, 551–569.
Tornos, F., Barriga, F., Marcoux, E., Pascual, E., Pons, J.M., Relvas, J., Velasco, F., 2000. The Iberian Pyrite Belt. In: Large, R., Blundell, D. (Eds), Database on global VMS districts: CODES-GEODE, pp. 19–52.
Tornos, F., 2006. Environment of formation and styles of volcanogenic massive sulfides: the Iberian Pyrite Belt. Ore Geol. Rev. 28, 259–307.
Tornos, F., Heinrich, C.A., 2008. Shale basins, sulfur-deficient ore brines and the formation of exhalative base metals deposits. Chem. Geol. 247, 195–207. https://doi.org/10.1016/j.chemgeo.2007.10.011.
Van den Boogaard, M., 1963. Conodonts of Upper Devonian and Lower Carboniferous age from Southern Portugal. Geologie en Minjbow 42 (8), 248–259.
Vidal, O., Goffé, B., Arndt, N., 2013. Metals for a low-carbon society. Nat. Geosci. 6, 894–896.
Wang, J., Zuo, R., 2018. Identification of geochemical anomalies through combined sequential Gaussian simulation and grid-based local singularity analysis. Comput. Geosci. 118 (May), 52–64. https://doi.org/10.1016/j.cageo.2018.05.010.
Wang, W., Cheng, Q., Zhang, S., Zhao, J., 2018. Anisotropic singularity: a novel way to characterize controlling effects of geological processes on mineralization. J. Geochem. Explor. 189, 32–41.
Yang, J., Agterberg, F.P., Cheng, Q., 2015. A novel filtering technique for enhancing mineralization associated geochemical and geophysical anomalies. Comput. Geosci. 79, 94–104. https://doi.org/10.1016/j.cageo.2015.03.011.
Yilmaz, H., Cohen, D.R., Sonmez, F.N., 2017. Comparison between the effectiveness of regional BLEG and −80# stream sediment geochemistry in detection of precious and base metal mineral deposits in Western Turkey. J. Geochem. Explor. 181, 69–80.
Yousefi, M., Carranza, E.J.M., 2015. Prediction-area (P-A) plot and C-A fractal analysis to classify and evaluate evidential maps for mineral prospectivity modeling. Comput. Geosci. 79, 69–81. https://doi.org/10.1016/j.cageo.2015.03.007.
Zuo, R., 2011. Identifying geochemical anomalies associated with Cu and Pb-Zn skarn mineralization using principal component analysis and spectrum-area fractal modeling in the Gangdese Belt, Tibet (China). J. Geochem. Explor. 111 (1–2), 13–22. https://doi.org/10.1016/j.gexplo.2011.06.012.
Zuo, R., Wang, J., 2016. Fractal/multifractal modeling of geochemical data: a review. J. Geochem. Explor. 164, 33–41. https://doi.org/10.1016/j.gexplo.2015.04.010.